AD-A047 472 STATE UNIV OF NEW YORK AT STONY BROOK DEPT OF MATERIA--ETC F/G 11/6
THE RESPONSE OF COATED STEELS TO CAVITATION IN CORROSIVE ENVIRO--ETC(U)
MAY 77 H HERMAN, C CLAYTON, S AGARWAL N00014-75-C-1018

UNCLASSIFIED TR-2 NL

| OF |
AD
A047472

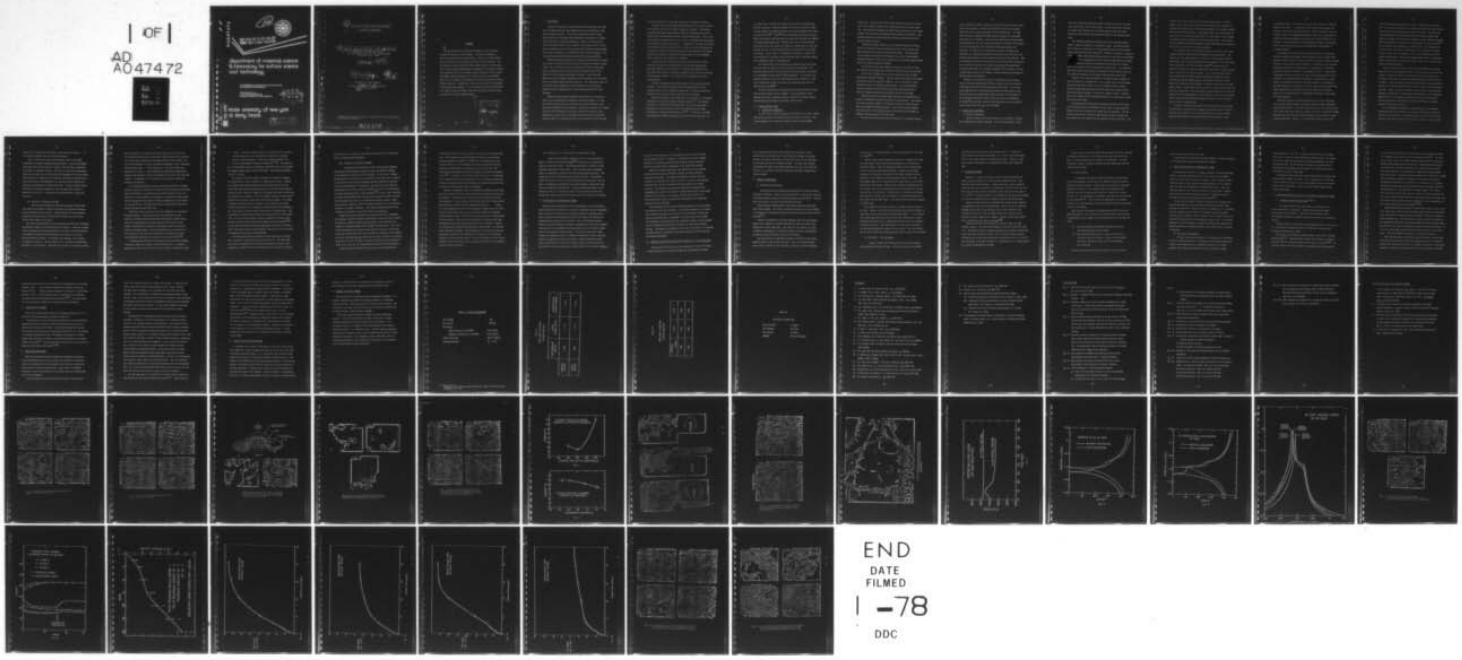

END
DATE FILMED
1-78
DDC

department of materials science & laboratory for surface science and technology

THE RESPONSE OF COATED STEELS TO CAVITATION IN CORROSIVE ENVIRONMENTS

Technical Report No. 2
To the Office of Naval Research
Contract No. N00014-75-C-1018, NR036-110

state university of new york at stony brook

(6)

THE RESPONSE OF COATED STEELS TO CAVITATION IN CORROSIVE ENVIRONMENTS.

(10) H./Herman, C./Clayton, S./Agarwal, S./Safai and J./Vargas

Department of Materials Science
The State University of New York at Stony Brook
Stony Brook, N.Y. 11794

(11) May 1977 (12) 62p.

(9) Technical Report No. 2.
to
The Office of Naval Research

(14) TR-2

Contract No. N00014-75-C-1018 NR036-110
(15)

401 074

LB

ABSTRACT

Cavitation-erosion in marine environments can have serious, deleterious effects on coated steels. This work is aimed at a detailed understanding of these effects. Studies are being carried out on aluminum-zinc alloy and alumina-base ceramic coatings. The resistance to corrosive media of these coated steels are being studied, with and without polyurethane impregnation of the porous coating, since polymer-filled flame sprayed anodic coatings are known to give remarkable corrosion protection in a range of marine environments. Details of the thermal spray process are also being examined as these effect properties. Furthermore, transition metal/metalloid amorphous coatings are being examined. It is our intent to study erosive/corrosive effects where, for modern, high velocity marine vehicles, they are cettain to play an important role.

I. INTRODUCTION

Protective coatings on steel by metals and oxides have for some time been applied by the rapid deposition and solidification of the molten coating material. Since the introduction of this thermal spraying process there have been considerable advancements in equipment design and in spraying techniques. However, there have been limited careful studies of the properties and microstructures of the coatings produced, and this has prevented the thermal spraying method from being recognized as a highly significant coating technique. Its versatile characteristics have thus not been fully appreciated.

Thermal sprayed aluminum and its alloys are well known for providing durable corrosion protection on steel structures (cathodic protection). The limitations as well as potentials of the aluminum-type coating, however, have not been seriously considered due to the absence of the relevant metallurgical studies. One of the main objectives of the present research has been to examine the microstructures of plasma-sprayed aluminum and Al-Zn. This represents a part of an ongoing research program at this laboratory on the corrosion properties and microstructures of thermal-sprayed metal and oxide coatings.

Thermal sprayed coatings typically have neither the structural density nor the mechanical strength of the cast structure. As such the nature of the porosity and interparticle bonding determine the mechanical properties of the coating. Whereas the porosity will largely determine the likelihood of long term corrosion protection of the substrate, so also will the resistance of the coating to cavitation erosion, which is a function not only of porosity but of the strength

of the interparticle and the coating/substrate interfacial bonding.

Aluminum and zinc have been used extensively in the past as protective coatings for steel structures exposed to seawater. The coating cathodically protects those areas of the steel substrate which are in contact with the electrolyte via the inter-connected pores. Zinc is the most effective coating, but it is expensive. We believe that the protective coatings of zinc may be improved by additions of aluminum for whilst the more highly anodic potential of zinc improves the throwing power of the coating, enhancing cathodic protection of the substrate, the marked reduction in porosity of the Zn-Al coatings points to an improvement both in corrosion and cavitation resistance.

Studies have been carried out on the structural nature of the Zn-Al coatings and the resultant forms of cavitation damage which have been achieved in these coatings. A preliminary study has also been made on the effect of cavitation damage on the corrosion resistance of the aluminum coatings. This work will be extended to the Zn-Al alloy coatings.

The major technologically-related aspects of the sprayed coating include: i) The coating-substrate adhesion mechanism(s) and the characteristics of the interfacial region and; ii) Particle-particle cohesion and the related "bulk" properties of the coating.

Relative to adhesion to the substrate, in spite of the considerable literature on the bond strength of sprayed coatings[1,2] the bonding mechanism is still not clearly understood. Of the many mechanisms proposed, mechanical bonding is generally considered as the major contributor to coating-substrate adhesion[3,4]. In practice, surfaces are prepared for thermal spraying by hard particle grit blasting. It

is thought that the high velocity grit both cleans and abrades the surface, creating a situation needed for effective mechanical interlocking between the sprayed particles and micro-irregularities of the roughened surface[5]. Apps[6,7] has investigated variations in grit blasting procedures and how these variations may influence the bonding of sprayed aluminum to steel. However, all such studies have been correlated mainly with mechanical adhesive strength and, as such, are related to complex experimental problems associated with the method of testing. In our view, it is important to examine in detail the microstructure of the first layer of coating that is applied, because this interfacial layer is the weak link.

The interbonding of the particles has received even less attention than that of adhesion of the coating to the substrate. The possible mechanisms for the cementation of the particles is expected to be dependent on the specific coating material. For example, for aluminum, sprayed in air, the rapid oxidation will result in a thin layer around each particle and this oxide must play some role in interparticle bonding[8].

In the following will be considered both the microstructural and the corrosion aspects of this program. The two portions of the program are given in separate sections, but the interaction between microstructure and chemical properties will be clear.

II. MICROSTRUCTURAL STUDY

A. EXPERIMENTAL PROCEDURE

In this study, aluminum coatings were sprayed in air with a Metco 3MB plasma gun under the spraying conditions given in Table I. The spraying powder was a spherical, nominally pure aluminum powder

(Metco-45). Cleaned, mild steel (1018) substrates were grit blasted with 750 μm angular alumina grits immediately prior to plasma coating. Substrate-free coatings were obtained by depositing a thin layer of NaCl (<5 μm) on the grit-blasted steel heated to over 100°C. The sprayed aluminum can be subsequently removed by the dissolution of the salt layer in water.

Aluminum coatings, 25x75 mm, were uniformly sprayed (75-750 μm thick) by traversing the gun mechanically while the specimens were kept stationary on a water-cooled aluminum block. The temperature of the sample was monitored continuously by a set of thermocouples attached through the back of the substrate and positioned approximately 200 μm from the grit-blasted surface.

In the case of the alloy study, the alloy, in the form of wire was electric arc-sprayed under conditions similar as for the aluminum.

As will be discussed later, it was required to obtain single particles of sprayed aluminum. This was achieved by passing the plasma gun quickly over the substrate surface. This is basically a splat quenching process, utilizing a plasma torch. The single droplets usually detach from the polished surface with no difficulty and could be studied directly by transmission electron microscopy.

Scanning electron microscopy (SEM) has been used extensively in order to characterize the bulk structure of the coatings. Top-surface and cross-sectional samples of aluminum were cut by a precision saw and then prepared metallographically. Some of the aluminum samples were etched with a 15%-sodium hydroxide solution and then washed in methanol before mounting on the SEM stud.

The pore structure and particle morphology in the coatings can be

studied with SEM; however, the grain size within the particles is too fine to be resolved. Therefore, transmission electron microscopy (TEM) was used to reveal the nature of the crystallites. For TEM, thin foils were prepared from 500 μm thick coatings, by mechanical polishing of cut sections. The foils were then further thinned either electrochemically (4 to 1 methonal-perchloric acid (70%) electrolyte), or by ion bombardment, until electron-transparent regions were obtained. To observe the microstructural changes throughout the thickness in a coating, and especially the grain-size variation with distance-from-substrate, cross-sectional cuts were also prepared. This last technique is particularly useful since the area under observation can be directly located in the coating by in situ TEM examination. To minimize heating in the samples prepared by ion thinning, very low voltages were used (2-3 KV); however, slight recovery was observed in TEM for some of the samples.

Finally, to characterize the pore structure of the coatings, mercury intrusion porosimetry (MIP) was combined with stereological information obtained from SEM and optical microscopy. It is to be noted that MIP does not necessarily present the true porosity, due to the existence of closed pores within the bulk of the coating. A vacuum-modified porosimeter with a pressure range of 0-50,000 psi (0-3.45x10^8 Pa) was used, and the values reported are the average of three or more tests for each set of samples.

B. RESULTS AND DISCUSSION

i) Particle Morphology

Surface cleaning and grit blasting of the substrate is essential preparatory to plasma spraying. It was realized early in this

study that substrate topography influences the structure of the coatings through means other than bonding. It was thus deemed important to examine the roughness of the substrate and its effects on the structure of the initial and successive layers of the aluminum coatings.

The impacting alumina particles used in grit blasting create a highly irregular surface on a microscopic level. The protuberances thus formed are responsible for the supposed mechanical interlocking between the coating and the substrate. Moreover, microscopic irregularities also effect the solidification behavior of the impinging particles.

he surface topography of the grit blasted substrate was examined

Substrate materials examined were mild steel and aluminum which were cleaned and grit blasted with alumina grit. For comparison, and also in order to determine the influence of the blasting angle on the surface morphology, two different blasting angles were used.

Figures 1 and 2 show SEM photos of the grit blasted surfaces of steel and aluminum, respectively. It is evident that for both metals blasting at 45° angle results in a directionally eroded surface, whereas perpendicularly blasted surfaces show mainly random craters, with some impacted regions in the center of these craters. Deformation of the surface of the aluminum substrate is of course more severe than that of the steel.

Considering only the mechanical bonding mechanisms, the blasted surface should ideally be composed of large number of deep undercuts through which the coating can be wedged into the substrate. The two criteria which are of importance and should be closely examined are the roughness of the surface and the geometry of the protrusions. The

appearance of flat regions on the blasted surfaces (Figs. 1 and 2) suggest that in order to obtain very rough surface and, therefore, to maximize the surface area on which the coating will be sprayed, smaller alumina grits should be used. Large grits result in a small number of deep undercuts, whereas blasting with finer grits gives a large number of shallower craters yielding an undulating appearance. The presence of large number of such protuberances insures good adherence by providing anchoring points for the sprayed coating.

On the other hand, blasting angle plays an important role in the formation and orientation of the protuberances on the surface. The lowering of this angle results in a decrease in the average depth of the craters, and at very low angles it merely results in the scratching of the substrate. Results obtained by Apps[6,7] indicate that the adherence strength of aluminum sprayed onto grit-blasted steel decreases with a decrease in the blasting angle. App's roughness measurements for various types of blasting grits consistently indicated rougher surfaces for the 60° blasting angles than those blasted at a right angle with respect to the substrate. Similarly, comparison of the SEM photos (Figs. 1 and 2) seems to also indicate an increased roughness for the lower angle (45°). The implication of such observations is that the geometry of the protuberances on a grit blasted surface is the decisive factor for good coating-substrate bonding, whereas surface roughness per se plays a secondary role.

To further illustrate the effect of grit blasting on the coating, solidification of the particles sprayed onto smooth and grit blasted surfaces were compared. On being injected into the plasma effluent particles are melted and accelerated towards the substrate. Upon

impingment onto the cold surface, they lose their kinetic and thermal energies and, therefore, experience ultra-rapid solidification, and concurrent high strain-rate deformation. Metallic particles, such as aluminum, under ideal spraying conditions, retain their plasticity for a sufficient time and generally conform to the local geometry of the surface. On the other hand, in high temperature oxides, due to their brittle nature, cracking occurs and considerable fragmentation is commonly observed.

On polished surfaces, however, both the aluminum and the oxide particles undergo considerable radial sliding, and the original semi-spherical molten droplet transforms into a linticularly shaped flattened particle, with a thicker middle section. A schematic of such particle morphology, based on our observation of a large number of particles sprayed onto polished surfaces, is presented in Fig. 3. Typical TEM micrographs of aluminum and alumina (ion thinned) particles are also included. An explanation for such behavior is that while the inter-facial areas between the particle and the substrate is solidifying, the upper regions of the particle is still molten, and because of high impact momentum the remaining molten region flows in a direction parallel to the substrate until the particle temperature drops below the freezing point.

Based on the grain orientation observed in the TEM micrographs, it is proposed that the heat extraction direction changes throughout the impinged particle. In the core region (Fig. 3), where the particle first comes into contact with the surface, the heat is extracted through the substrate, and the solid-liquid interface moves parallel and away from the substrate. However, in the peripheral areas, heat is not

extracted through the substrate but rather through the core region. This is clearly indicated by the radially elongated grains which propagate from the core and terminate at the rim portion. Actually, the virtually defect-free and regularly-patterned grains suggest that these thin regions are not fully in contact with the substrate surface. Similar arguments are presented in a recent paper by Wood and Sare[9] for the case of splat quenching of metal alloys. The assumption of one-dimensional heat flow, perpendicular to the substrate was shown in their study to be unreasonable. The present TEM observations of plasma-sprayed aluminum particles strongly support their experimental results regarding the "parallel" heat flow in the thin regions of the liquid-quenched particles.

These observations are not limited to small particles, but have been noted in larger droplets as well. In this case, however, the core region is larger and usually too thick to be examined by TEM in the as-sprayed condition. It should be emphasized that not all particles solidify in such symmetrical geometry, and, depending on the particle's initial size and configuration at the time of impact, different shapes may form. However, the basic liquid flow and solidification behavior appears to be the same. Furthermore, solidification in the elongated grains of metals is usually continuous and results in long single grains, whereas the oxide particles usually solidify by successive nucleation and growth (Fig. 3c).

On a grit-blasted surface the sliding process is considerably limited and one would therefore expect grain morphologies similar to that of the core region. The removal, without deformation, of single particles from grit blasted surfaces was not feasible. However, this

problem was overcome by examinations of the particles directly within the coatings sprayed onto a grit-blasted surface.

In Fig. 4 are given three cross-sectional views of the grain morphology in a plasma-sprayed aluminum coating. A typical micrograph of an area near the top surface is shown in Fig. 4a where, generally, the grains are randomly oriented. Particles in this region experience lower cooling rates and are effected by the topography of the previously deposited layers. Deeper into the coating, the grains become directionally oriented and the elongated axis is usually directed towards the substrate to which heat is flowing (Fig. 4b). Finally, columnar grains are observed immediately adjacent to the substrate which grow in a direction normal to it. They appear to be equiaxed from a plan view (Fig. 4c).

ii) Structure of Aluminum Coatings

The bulk microstructure of the plasma-sprayed aluminum coatings consists of lamellar structure formed by the flattened platelets of the individual metal particles. SEM micrographs of these droplets, sprayed on polished and grit blasted steel surface, are seen on the initial layer shown in Fig. 5a, b.

The rapid solidification of these impinging particles will influence the particle-substrate and particle-particle bonding. Therefore, sprayed aluminum coatings are complex aggregates of partially sintered particles with numerous structural discontinuities which result in low interparticle cohesive strength. In addition, the coatings, for a variety of reasons, are porous. The porosity will act to degrade the mechanical properties of the coatings. Such pores can be seen in the cross-sectional

SEM micrograph of a polished and etched aluminum coating (Fig. 5c). The excessive etching of the interfacial region indicates the presence of a region more chemically active than the bulk of the coating. An electron microprobe analysis of the aluminum sprayed on steel indicated an interfacial layer of approximately 3 μm. The exact nature and composition of this thin layer could not be conclusively determined. However, grit blasting is generally thought to "activate" the substrate surface. In addition, it is likely that the interface contains an "aluminum iron oxide".

The true pore geometry can not be readily identified in aluminum coatings because such coatings are generally soft and deform plastically during preparation. Such deformation is clearly evident in Fig. 5c. Therefore, a cross-sectional micrograph of a polished and etched oxide coating (Al_2O_3-13% TiO_2 etched in boiling orthophosphoric acid (85%)) is included in order to demonstrate the pore morphologies observed in typical sprayed coatings (Fig. 5d).

Generally, there are two types of pore geometries in the plasma-sprayed coatings: (i) elongated pores, mostly parallel to the substrate, formed between the particles (occasionally some of these pores are interconnected, forming a network which results in the typical laminated-like structure); (ii) pores, nominally spherical, formed by entrapped gases. Both pore geometries are illustrated in Fig. 5d; however, the small verticle cracks are thought to be due to preferential etching of the cracks in the oxide particles[10].

Scanning electron and optical microscopy can furnish considerable information about the structure of the internal pores. To obtain a quantitative measure of the overall volume fraction of these pore, MIP

was employed. The total volume and the size distribution of the open surface-connected pores were determined as a function of spraying distance and coating thickness. These two spraying parameters are known to have considerable influence on porosity[11,12]. The pores in all of the coatings which were examined ranged from 0.01 to 10 μm, with the highest number being in the 1-4 μm range. The total pore content is given in Fig. 6.

As expected, the pore content increases with spraying distance. The implication of such an increase is simply that at large distances (e.g. 250 mm) the spraying efficiency for aluminum declines to the extent that good bonding between particles can not take place, and the coating formed is simply an aggregate of loosely held aluminum particles, with large pores in-between. The main factors involved are the partial solidification prior to impact and loss of kinetic energy. The slight increase in porosity at lower distances is attributed to the superheating of aluminum and the tendency to absorb gases, mostly hydrogen, as is well known, into the molten droplets before solidification. SEM examination of such coatings points to the presence of sub-micron pores (.01 - 0.1 μm) in some regions, forming a sponge-like microstructure. A similar observation has been made in Al_2O_3 coatings by Koubeck[13], who has shown that with excessive hydrogen gas in the flame, and therefore a large heat content, molten droplets undergo partial vaporization, and produce porous areas on solidification.

The influence of coating thickness on the porosity was examined over a thickness range from 0.45 to 1.2 mm (Fig. 7). The total open pore volume decreased with the increase in thickness; however, this variation is rather small and is considered to be caused by the larger

contribution of the internal closed pores to that of the surface pores which are measured by porosimetry.

iii) Oxidation in Aluminum Coatings

Interaction of the particles with the surrounding gaseous environment during spraying is known to exert considerable effects on the bonding and structure of the coatings. In the case of plasma-sprayed aluminum, sprayed in air, oxidation of the particles in transit to the substrate can greatly influence the post-impingement particle-particle interdiffusion. Furthermore, the oxide skin which forms on each particle will likely restrict flowability prior to solidification, and thus increase porosity. Mash and Brown[14], using a water immersion technique (ASTM C20-46) have examined the porosity of aluminum coatings plasma sprayed in air and in a controlled atmosphere chamber. They have reported a density of 76% for aluminum sprayed in air, and 86% for spraying in an argon atmosphere. This large difference points to the important contribution of the oxide film on the porosity.

Oxide layers were detected on the flattened particles throughout the coatings, and TEM examination indicated that the oxide skin, formed on particles, usually fractures during impact on the substrate and remains as scattered patches on the larger aluminum grains. Fig. 8a is a TEM micrograph of such an area from within the coating, showing the ultra-fine crystallites which yield diffuse SAD. Heating of such regions by the electron beam <u>in situ</u> within the microscope resulted in crystallization of the film: The same area after 15 minutes of beam exposure is shown in Fig. 8b, with its corresponding electron diffraction pattern.

Some areas were occasionally noted where grain morphology was

considerably different from the normal structure of the aluminum coatings. These regions were mostly within the bulk of a coating and contained grains much smaller (~750 Å) than the average grain size usually observed. A TEM micrograph of such a polycrystalline area, prepared by electrochemical polishing, is seen in Fig. 8c. The corresponding SAD pattern correlates closely with metastable aluminum oxides[15]. Therefore, it is believed that these areas are formed by local oxidation of the aluminum particles in the turbulent plasma gas. However, such observations were limited, and surface oxidation is more prevalent in plasma sprayed aluminum coatings.

Another consideration which is pertinent to oxidation in aluminum coatings is the role of the oxide film on the mechanical properties of the coating. The low cohesive strength of aluminum coatings can be attributed to: i) the presence of a brittle oxide film at the particle boundaries which impedes particle interaction and can act as a path for crack propagation; and ii) the existence of large numbers of interparticle pores which reduce the surface area between the particles forming "bottle-necks", and therefore increase the stress concentration in these regions. Cracks can be nucleated at the pores and can then propagate through the oxide layers, giving rise to failure. Figure 9 is a micrograph of substrate-free-aluminum coating which was fractured under three-point bending. The delamination of the lamellae along the boundaries, parallel to the substrate, is evidence for the particle boundary fracture discussed above. After delamination the still intact layers of particles fail both by interparticle debonding and by ductile fracture within a particle.

iv) Al-50 wt.% Zn - A preliminary microstructural study

Three different phases; namely pure Zn, Al and intermediate phase $\acute{\alpha}$, identified by Rao and Herman[16], were found in sprayed Al-Zn alloy by x-ray diffraction. The diffraction pattern is similar to the quenched alloy aged at about 100°C. This indicates that the sprayed alloy is decomposed by subsequent heating during spraying process. The morphology of the decomposed alloy was studied by TEM. Precipitates within the matrix as well as at grain boundaries are observed. Fig. 10 shows a discontinuous precipitate at a grain boundary, which grows into the supersaturated solid solution. A matrix precipitate phase is also observed in Fig. 10. Of interest here is the occurrence of free zinc precipitate, which we believe will play some role in corrosion resistance.

C. COMMENTS ON THE MICROSTRUCTURAL STUDY

Emphasis has been placed here on the fundamentals of the solidification process of the particles and the role of substrate surface topography. Using methods of transmission and scanning electron microscopy we were able to observe the ultrastructure of the first layer and, thereby, to synthesize the process of its formation. On a grit-blasted surface, where there exist numerous microscopic irregularities, the molten aluminum droplets will be constrained by surface asperities, thus limiting radial flow from the center of the particle. The particles striking a rough surface are therefore smaller in diameter and generally thicker than the particles sprayed onto a polished surface. TEM observations indicate that such particles are made up of columnar grains oriented parallel to the direction to which heat flows. Directionality of the grains disappears

in the mid- and upper-layer of the coating, where the cooling rates are considerably lower. In general, the morphology of the impinged particles is effectively controlled by particle-size and location within the coating and the topography of the underlying surface.

The process-induced porosity in the coatings may be reduced by optimizing the spraying parameters; however, porosity cannot be completely eliminated. Porosimetry measurements indicate that for aluminum, the dominant pore size is in the 1-4 μm range, the spraying distance being the most influential control parameter in overall porosity. The prevalent pore geometry observed was interparticle-elongated pores with the long axis of a pore being mainly in the planar surface of the coating. The presence of such pores hinders the particle-particle cohesive bonding and thus degrades the mechanical properties of the coatings.

The interaction of the molten aluminum droplets with the surrounding environment was also examined. For coatings sprayed in air, excessive oxidation may occur which limits the interdiffusion between the metallic particles after impingement. The oxide layer also reduces the flowability of the particles and, therefore, higher kinetic energies must be imparted to the particles in order to attain good cohesive bonding. In general, the presence of such thin oxide layers in a sprayed aluminum coating is detrimental and can be avoided by controlling the surrounding atmosphere.

III CORROSION AND CAVITATION BEHAVIOR OF SPRAYED Al and Zn-15 wt.% Al

The protection afforded by sprayed coatings of Al and Zn-Al alloy in NaCl solution was investigated using the electrochemical method.

This involved measuring the time change in the potential of the system formed by the base metal (steel) and the sprayed coating for coatings of various thicknesses, and also the open circuit potentials of the steel and the free sprayed coatings. The next step involved determining the anodic polarization behavior and, thus, the corrosion current, i.e. current of the pair formed by base metal (cathode) and coating (anode).

A. CORROSION EXPERIMENTS

i) Open Circuit Potentials

Corrosion potential measurements were made on aluminum in three different conditions: namely; (1) Cast and rolled - high purity aluminum; (2) Plasma-sprayed aluminum; (3) Plasma-sprayed Al-coated steel. Table II shows the results in aerated and deaerated solutions.

Plasma sprayed aluminum shows a more active potential than cast and rolled aluminum. The shift in corrosion potential is due to absence of segregation of impurities because of the splat-quenched nature of this material[17].

Further, the potential of system formed by steel and the sprayed layers falls between the initial potentials of steel and that of the sprayed metal taken separately. The steel and the coating may, thus, in effect be considered as a bimetallic system closed by electrically conducting medium through the pores of the coating..

The materials in the deaerated solutions establish a more active potential than in the aerated solutions. This is in agreement with other results reported in the literature, because in aerated solutions

an oxygen cell is extablished which shifts the potential in the noble direction[18].

Similar results were observed in electric arc sprayed Zl-Al coating, where open circuit potentials were measured as a function of coating thickness. Table III shows the effect of the coating thickness and the gun current during spraying. Cathodic polarization increases with increasing thickness of the anodic coating, and the potential of the bimetallic system approaches that of the steel. It would appear that with increased thickness, more steel is coming into contact with electrolyte. However, this contradicts expectation, for this assumes that the through-porosity may be concluded to be increasing, but this is not likely. Alternatively, the aluminum coating may be becoming less anodic, due, for example, to increased oxidation of the coating for the outer layers. This will be more carefully examined in further work.

The situation is reversed, however, if higher spraying currents are used. Whereas, the potential becomes more noble with thickness, at higher gun currents the potentials become more anodic. It is expected that higher quenching rates are obtained with increased gun currents because the traverse time is reduced and droplets strike the substrate at higher velocities. This would increase the amount of retained $\acute{\alpha}$ and therefore decrease the amount of free aluminum. This may account for the shift to the more anodic potentials with increase in gun current.

ii) Potential - Time Dependence

Figure 11 shows that the potential of the steel-aluminum system becomes positive with time. This may be due to the aluminum

coating gradually dissolving, thus exposing steel, as a result of which cathodic polarization decreases. Or, it may be that the properties of the sprayed coating are changing with time. However, in the Zn-Al system, the potential is exceptionally stable with respect to time.

B. POLARIZATION PLOTS

Figures 12, 13 show the results of polarization measurements of plasma sprayed aluminum and of the aluminum coating on steel. Both materials show similar features. Anodic plots show a sharp change in anodic current as the potential is shifted from -0.75 to -0.70v vs S.C.E. This rise of anodic current corresponds to the onset of pitting due to Cl^- ions[19]. Pitting potential is not affected by the processing method, since the same potential value is shown by cast and rolled aluminum.

However, higher currents are obtained with plasma-sprayed aluminum as compared with cast and rolled aluminum. This is due to two factors: Coatings, due to their rough surface, have a higher effective area exposed to solution for the same sample size; and, secondly, due to presence of pores, added area is exposed. Another contribution may be due to chloride ion build-up in the pores[20].

Cathodic plots for all the materials show that they are under cathodic control. The diffusion of oxygen is the main controlling reaction. Polarization plots of sprayed coatings and of sprayed coating with steel show that a very small area of steel is actually being exposed. Therefore, the current contribution due to dissolution of iron is not at any significant level and, if there is a contribution, it is being dwarfed by currents established by aluminum.

Figure 14 shows the polarization plots obtained with Zn-Al coatings of different thicknesses. It is evident that polarizability of the alloy is significantly lower than that of pure aluminum. For both thicknesses studied, corrosion currents are much higher than for the aluminum-steel system.

i) Mode of Attack

To determine the type of attack suffered by coatings below the pitting potential, coated steel was exposed at anodic potentials below the pitting potential. Attack seems to be confined to particle boundaries and pores in the coating, where the concentration of chloride ions will be greater and attack will thus be more severe: See Fig. 15. Grain boundaries are normally delineated in cast aluminum at this potential[21]. This confirms the hypothesis that sprayed materials are very homogenous, and the exceptional corrosion resistance is due to this effect.

Good corrosion resistance of plasma-sprayed materials has here been demonstrated. Very significant conclusions can be made from the electrochemical results about the two sprayed materials, aluminum and Zn-Al.

(i) The electrochemical protection afforded to steel by the aluminum coating is only slight.

(ii) Electrochemical protection is much more effective in the case of the Zn-Al system. However, these coatings have higher dissolution rates and will be attacked more uniformly.

The role on corrosion protection of steel of any free zinc is

uncertain for the Zn-15 wt.% Al alloy.

Future work will examine this possible effect of α'-phase retention in the higher gun current arc-sprayed Zn-Al alloys.

C. EFFECTS OF CAVITATION ON CORROSION IN 5% NaCl

Cavitation and corrosion, if present together, can have disastrous effects, even when either process may not be particularly harmful. Interaction will vary from system to system. Under cavitation conditions the passive layer cannot be sustained because it will crack or spall off under the influence of the cavitation stress. Also, the cavitation process will effect the kinetics of the cathodic reaction, when gasses are evolved or absorbed because of turbulance and the formation of bubbles associated with cavitation[22].

To note the synergistic effect of cavitation and corrosion, the polarization behavior of pure aluminum coatings was studied in the presence of cavitation. Besides the shift in potential, it is observed that the cathodic current values are increased, though the anodic currents are not effected. This is shown in Fig. 6, where currents at three different potentials are measured at various times. At cathodic potentials, a sharp increase in current is observed when cavitation is impressed; while at an anodic potential, very little change in current is observed.

i) Weight-Loss Measurements

To study the corrosion behavior in the presence of cavitation, weight-loss measurements were carried out at four different potentials: at open circuit potential; at a cathodic potential; at an anodic potential less than pitting potential; and at a potential beyond

pitting potential: Fig. 17. At open circuit potential, the weight-loss curve is similar to that observed in distilled water. An incubation time is generally obtained in cavitation experiments, but none was observed here. At all potentials, except for potentials more noble than pitting potentials, the weight loss rates are within the experimental scatter of each other.

At potentials more noble than the pitting potential, however, one observes higher weight loss rates. This is because pits created due to electrochemical attack will act as preferential sites for material removal due to cavitation. This will lead to higher weight losses at these potentials.

IV. CAVITATION DAMAGE OF Zn-15 wt.% Al ELECTRIC ARC-SPRAYED COATINGS

A. INTRODUCTION AND PREVIOUS WORK[23a,b,c]

As indicated previously, the behavior of Al-base Zn in a marine environment is uncertain. Added cavitation-erosion makes things still more difficult. It was thus felt imperative that a metallographic study be conducted, related to corrosion and cavitation-erosion.

An alloy which has received much engineering attention is Zn-15 wt.% Al. We have thus examined Zn-15 wt.% Al from both a corrosion and cavitation-erosion point of view.

Previously, Fauty studied cavitation-erosion properties of thermal sprayed Al_2O_3[23c]. Dakshinamoorthy studied the influence of alloying and grain size on cavitation-erosion of Cu-Ni and Cu-Zn alloys[23b]. In a previous report from this program it was pointed out that because of

the rapid weight-losses initially observed during cavitation-erosion, it is apparent that particle-particle bonding is weak[23]. The fact that a hotter flame and a higher velocity improves particle-particle bonding lends support to this conclusion. Though fracture can occur as either trans- or inter-particular, it is probable that in both cases the crack path is inter-granular, again due to weak particle-particle cohesion. Cavitation occurs because of the collapse of a large group of bubbles, creating a large burst of pressure which causes macroscopic deformation at the surface. It is also to be noted that incubation periods, usually associated with the cavitation erosion of the basis metal, is not present in a sprayed coating. This occurs since the scratch-free metal requires a period in which undulations on the solid surface are produced, which later become sites for weight loss. In thermal sprayed coating, however, weight-loss occurs immediately in the process and increase with exposure[23,24].

Dakshinamoorthy concluded that microstructural details (e.g. structure, grain size, solid solution formation, and second phase particles) play a major role in determining the resistance of ductile materials to plastic deformation. Since the grain size has a significant effect on the mechanical properties, it was anticipated that this parameter would also play a major role in determining cavitation-erosion resistance. It is in fact known that reducing the grain size increases erosion resistance. This will likely be a factor in intra-particle erosion.

Vyas concluded that, although the mode of stressing in cavitation is essentially repetitive and the total damage produced is cumulative, thereby fulfilling the definition of 'fatigue', the manner in which the material is damaged and subsequently fails is very different from that

produced by conventional (e.g. monotonic tensile/compression or bending) fatigue. Vyas thus feels that one should not, therefore, expect any direct correlation between fatigue strength and resistance to cavitation-erosion. He feels, from the data, that a correlation with resistance to explosive deformation would be more realistic[23a]. This conclusion will be considered in light of our present results on coatings.

B. EXPERIMENTAL TECHNIQUES

The present coatings were electric arc sprayed by Metco Inc., L.I., New York; spraying parameters are given in Table IV.

The Zn-15 wt.% Al alloy coatings were exposed to cavitation-erosion damage produced by a vibratory system consisting of an acoustic horn operated at a frequency of 20 KHz. The distance between the horn and the surface of the coatings was approximately 500 μm ±25 μm. The spacing is constantly changing but this is acceptable since there is a large enough range such that cavitation is negligibly effected by this slight change in spacing[23]. These experimental conditions were selected since they have been found to be optimum[23,24].

C. RESULTS AND DISCUSSION

Before any cavitation-erosion studies were performed, preliminary x-ray diffraction work was carried out on the sprayed alloy coatings. These are an indication, not surprisingly, that some phase separation has occurred in the as-sprayed coating. Further work is underway, using both x-ray and TEM techniques, to examine the phases present and their relative amounts.

The total weight loss curves obtained all show an initial rapid

weight loss region followed by a weight loss plateau. A comparison of these curves for different spray parameters (Fig. 18a-d), clearly indicates that the weight loss is greatest for the 0.006 inch thick coatings. The leveling-off is associated with complete removal of the coating. Thus, final leveling of the curves corresponds to the initiation of substrate erosion (This likely corresponds to the previously observed incubation time with no coating.). In fact, SEM micrographs show that in this region the grit blasted surface of the substrate has been reached.

The mechanisms of cavitation erosion of the coatings will now be discussed. Figure 19a is an SEM micrograph of an as-sprayed surface, typical of the surfaces found for all conditions. Here, platelets are surrounded and partially covered with particles which resemble spraying debris. After 30 seconds of exposure to cavitation, as indicated, this particle debris appears to be removed, leaving smooth platelets (Fig. 19b). The removal of the debris requires little cavitation exposure, suggesting that it is weakly bounded to the coating. In Fig. 19b, this surface is seen, along with some evidence of the fatigue-like fracture of the particle edges previously mentioned. As was stated above, the thin edges around the platelets and the sharp edges around pores are the primary areas of attack by cavitation-erosion. In fact, the oxides which are located at these regions will enhance failure. This is consistent with previous observation of particle delamination under 3-point bending (Fig. 9). This further deterioration of the coating is seen in Fig. 19c and d, for 60 secs and 3 minutes, respectively, of cavitation.

Fig. 20a shows that the failure after 5 minutes becomes similar to the columnar particle failure described by Fauty[23c]. Figure 20b is a

is a high magnification which illustrates the propagation of a trans-particle crack which originates from a sharp corner of a pore and propagates in a jagged manner along the grain boundaries. Figure 20c is for an advanced state of erosion, where the coating is virtually gone. Only well-adhered particles remain. Figure 20d is a high magnification of one surviving particle, clearly showing grain boundary attack. Figs. 20 c and d reveal what appears to be delineated grain boundaries. This may be due to localized erosion at these sites. It has been shown[23b] that grain boundary attack occurs in zinc. Dakshinamoorthy[23b] found that attack is typified by cracks initiated predominantly at grain boundaries propagating along the basal planes. This form of erosion is not found in FCC structures and may account for its absence in aluminum-sprayed coatings. Because this mechanism is only apparent in the last remaining coating particles, it would appear that this mechanism is a secondary form of damage to coatings of this type.

D. STATUS OF THE CAVITATION STUDIES

A comparison of the overall performance of the Zn-Al alloy coating with commercial, rolled aluminum shows that the alloy coating has lower cavitation-erosion resistance. It is anticipated that studies of this system will give greater insight into thermal spraying generally. The details of the mechanisms of cavitation-erosion damage are still elusive. However, the present results point to mechanisms involving particle-to-particle debonding. A careful study, involving both TEM and SEM, will form the next stage of this program. Particle analysis, we anticipate, will aid in a clearer understanding of what is occurring in these erosive

processes. Other materials (as coatings and substrates) as well as the influence of concurrent corrosion will be explored as well.

V. PROPOSAL FOR FUTURE STUDIES

This program will be oriented towards two general directions: i) a number of thermal spray methods and process controls; ii) different coating materials. These two areas are of course closely related. The principal issues under study are corrosion in a marine environment and cavitation-erosion, taken alone and together.

In the next research period we propose to greatly extend the program. It should be noted that the range of materials is being extended beyond that originally proposed for this program. It is important, however, to recognize recent developments in the field of materials science - i.e. amorphous alloys. Thermal spraying represents "applied splat quenching", and, as such, enables the formation of highly metastable structures. This viewpoint is being taken here, and it is further anticipated that these metastable structures will have particularly interesting and useable properties.

TABLE I - SPRAYING PARAMETERS[a]

Arc Voltage	60V
Arc Current	500 Amp.
Plasma gas	
Argon (Primary) @ 6.9×10^5 Pa	4.245 m^3/Hr.
Hydrogen (Secondary) @ 3.45×10^5 Pa	0.1415 m^3/Hr.
Powder feed rate	38×10^{-3} Kg/Min.
Spraying distance	10 - 15 cm

[a]Parameters for aluminum Powder (44-88 μm), Metco Al-54, Metco Inc., Westbury, L.I., N.Y.

TABLE II

OPEN CIRCUIT POTENTIALS

(1M NaCl SOLUTION)

	CAST AND ROLLED ALUMINUM	STRIPPED ALUMINUM COATING	ALUMINUM COATING ON STEEL SUBSTRATE
DEAERATED SOLUTION	- 0.96	- 1.175	- 1.195
AERATED SOLUTION	- 0.85	- 1.110	- 1.115

TABLE III

OPEN CIRCUIT POTENTIALS

(1M NaCl SOLUTION)

THICKNESS / CURRENT	0.003"	0.006"
200A	1.345	1.388
500A	1.290	1.366

TABLE IV

ARC SPRAYING PARAMETERS

WIRE FEED RATE	16 Kg/hr.
AIR PRESSURE	$3X10^5$ pa.
ARC VOLTAGE	24 Volts
CURRENT	500 and 200 amps.

REFERENCES

1. D. Davies and J.A. Whittaker, Met. Rev. 12 (1967)15.
2. E. Bardal, et al., Brit. Corros. J., 8 (1973)15.
3. H.A. Matting, H.D. Steffens, Metall., 17 (1963) 583, 905, 1213.
4. L.H. Van Vlack, "Metals/Materials Congress", Phil., Pa., (1964), Tech. Rep. No. P(10-1-64).
5. D.G. Vadivasov et al., Sov. Powder Met. and Metal Ceram., 93 (1970)12.
6. R.L. Apps, Inst. Welding, Metal Spraying and Plastic Coating Conf., London, May (1967), pp. 15-23.
7. R.L. Apps, J. Vac. Sci. Technol., 11 (1974) 741.
8. H.S. Ingham and A.P. Shepard, Metco Flame Spraying Handbook, Vol. III, Metco Inc., N.Y., (1965), pp. 21.
9. J. Wood, I. Sare, Met. Trans. A, 6 (1975)2153.
10. S. Safai and H. Herman, to be published.
11. D.M. Karpinos, Sov. Powder Met. and Metal Ceram. 140 (1974) 41.
12. S. Yu Sharirker et al., Sov. Powder Met. and Metal Ceram. 73 (1969)38.
13. F.J. Koubeck, Proc. 3rd Annual Scanning Electron Microscopy Symp., IITRL (1970).
14. D.R. Mash and I.M. Brown, Metals Eng. Quart., 2 (1964)18.
15. V. Wilms and H. Herman, Conf. Prec. 8th Int. Met. Spraying Conf., Sept., (1976), Miami, Florida.
16. K.K. Rao and H. Herman, J. of Inst. of Metals, 94 (1966) 420.
17. A.P. Bond, et al., J. of Electrochemical Soc., 113 (1966) 773.
18. Wilson Lynes, J. of Electrochemical Soc. Vol. 103, No. 8, p.467, 1956.
19. H. Bohri and H.H. Ohlig, J. of Electrochemical Soc. 116 (1969) 906.
20. G.W. Walter, Corrosion Sc., 16 (1976) 573.

21. J.R. Galvele and S.M. De Micheli, 10 (1970) 795.

22. Plesset, M.S., Corrosion, 18 (1962) 181.

23. SUNY at Stony Brook, Materials Science Department, Theses:

(a) "Cavitation Erosion of FCC Metals", Ph.D. thesis, B. Vyas, 1975.

(b) "Influence of Alloying and Grain Size on Cavitation Erosion Resistance", M.S. thesis, S. Dakshinamoorthy, 1976.

(c) "Cavitation Erosion of Plasma Sprayed Al_2O_3", M.S. thesis, J.K. Fauty, Jr., 1975.

24. "The Response of Coated Steels to Cavitation in Corrosive Environments", Technical Report No. 1, ONR, Contract No. N00014-75-C-1018, NR036-110, May, 1976.

FIGURE CAPTIONS

Fig. 1 - Surface of mild steel substrate grit blasted with Al_2O_3 at 45° (a,b) and 90° (c,d).

Fig. 2 - Surface of aluminum substrate grit blasted with Al_2O_3 at 45° (a,b) and 90° (c,d).

Fig. 3 - Schematic diagram of a particle after impinging onto a flat surface (a). Transmission electron micrograph of particle sprayed onto polished surface; aluminum (b) and aluminum oxide particle (c).

Fig. 4 - Cross-sectional grain morphology in sprayed aluminum coating showing the equiaxed grains near the top (a), partially oriented inside (b), and elongated, directionally solidified regions near the substrate (c). Arrow indicates the normal to the substrate surface.

Fig. 5 - Scanning electron micrographs of aluminum particles sprayed onto a flat surface (a) and grit blasted substrate where particle is observed to be restrained between the asperities (b). Cross-sectional view of coatings; polished and etched aluminum (c) and Al_2O_3-13 wt% TiO_2 (d).

Fig. 6 - Pore content of aluminum coatings measured by mercury porosimetry; total porosity vs. spraying distance.

Fig. 7 - Pore content of aluminum coatings measured by mercury porosimetry; total porosity vs. coating thickness.

Fig. 8 - TEM micrographs of a plasma-sprayed aluminum.

a) Ultra-fine crystalline oxide film with corresponding diffuse electron diffraction pattern.

b) Same area as (a) after 15 min. under the electron beam.

Fig. 8 -

c) Electrochemically-thinned polycrystalline region with a diffraction pattern corresponding to metastable aluminum oxides.

Fig. 9 - Scanning electron micrograph of a fractured aluminum coating (3-point bending test). The substrate's location in Figs. 6a, b is in the bottom and left-hand side, respectively.

Fig. 10 - TEM micrograph of sprayed aluminum-zinc alloy showing the second phase precipitate.

Fig. 11 - Potential vs. time plot for Al-steel and Al-Zn-Steel system.

Fig. 12 - Polarization plot for sprayed Al in 1M NaCl.

Fig. 13 - Polarization plot for Al coated steel in 1M NaCl.

Fig. 14 - Polarization plot for Al-Zn coated steel in 1M NaCl.

Fig. 15 - (a) Optical micrograph of corroded Al coated steel in 1M NaCl showing attack on particle boundaries.

(b) Showing attack on pores.

(c) SEM micrograph of corrosion product in a pore.

Fig. 16 - Current vs. time plot for Al coated steel with and without cavitation.

Fig. 17 - Weight loss curves under cavitation at different potentials.

Fig. 18 - Weight loss vs. time plot under cavitation for Al-Zn sprayed steel: (a) Coating thickness .006", arc current 200 amps.

(b) Coating thickness .003", arc current 200 amps.

(c) Coating thickness .006", arc current 500 amps.

(d) Coating thickness .003", arc current 500 amps.

Fig. 19 - SEM micrographs of sprayed Al-Zn coated steel under cavitation. (a) as sprayed coating showing loosely bonded particles; (b) after 30 secs of cavitation; (c) 60 secs of cavitation; (d) 3 min. of cavitation.

Fig. 20 - SEM micrographs of sprayed Al-Zn coated steel after (a) 5 min. of cavitation; (b) 10 min. of cavitation.

PUBLICATIONS DURING LAST CONTRACT PERIOD

1. "Plasma Spraying of Al_2O_3 and Al_2O_3-Y_2O_3", V. Wilms and H. Herman, presented at the "International Conference on Metallurgical Coatings", San Francisco, California, April 5-8, 1976: Thin Solid Films, 39 (1976) 251-262.
2. "Influence of Cavitation on the Corrosion Behavior of Plasma-Sprayed Coatings", S. Agarwal and C.M. Preece, TMS-AIME Fall Meeting, Niagara Falls, Sept. 1976.
3. "Microstructural Investigation of Plasma-Sprayed Aluminum Coatings", S. Safai and H. Herman, presented at the "International Conference on Metallurgical Coatings", San Francisco, California, March 28-April 1, 1977. To be published in Thin Solid Films.
4. V. Wilms and H. Herman, Conf. Proc. 8th Int. Metal Spraying Conf., Sept. (1976), Miami, Florida.

Fig. 1 - Surface of mild steel substrate grit blasted with Al_2O_3 at 45° (a,b) and 90° (c,d).

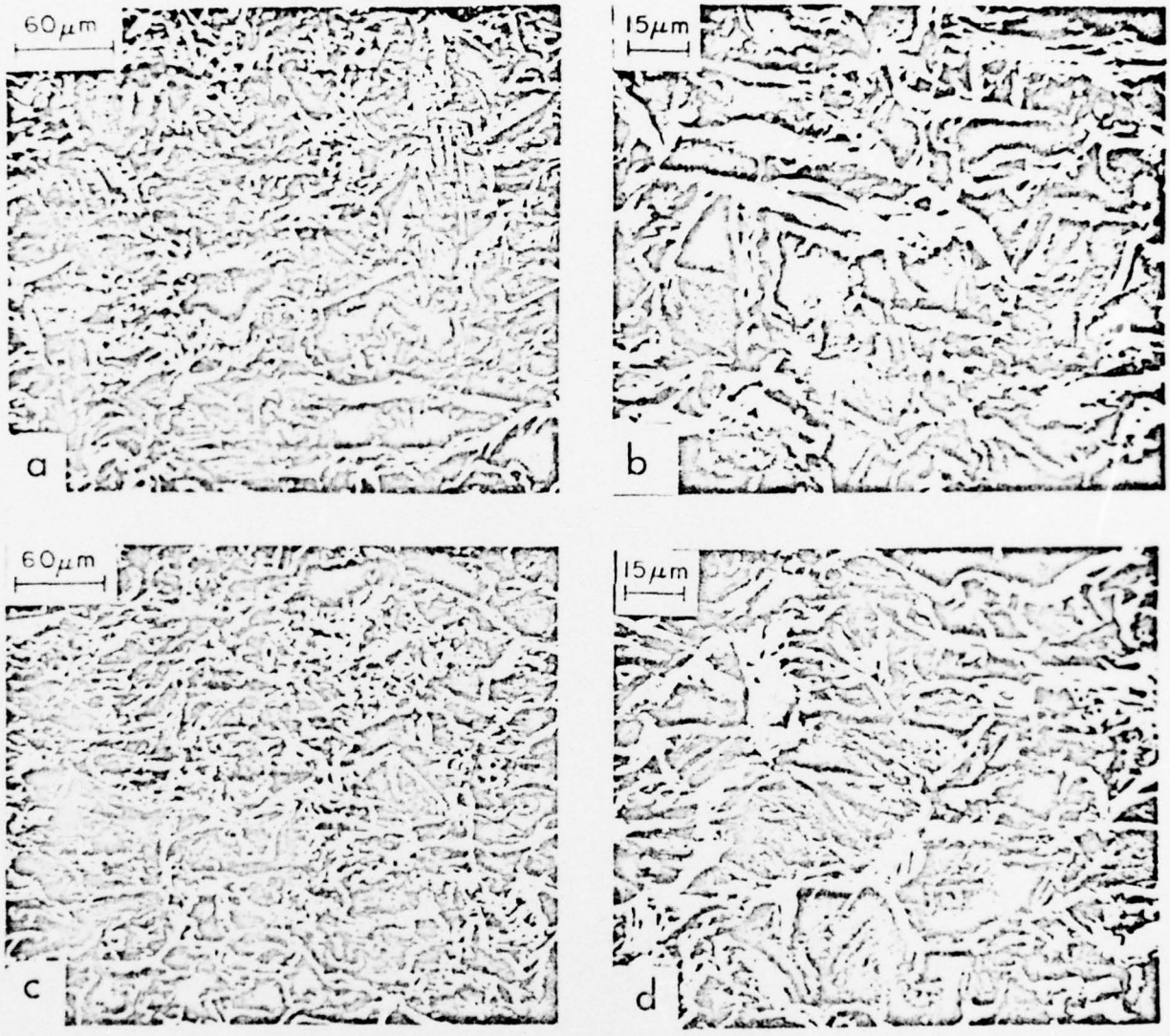

Fig. 2- Surface of aluminum substrate grit blasted with Al_2O_3 at 45° (a,b) and 90° (c,d).

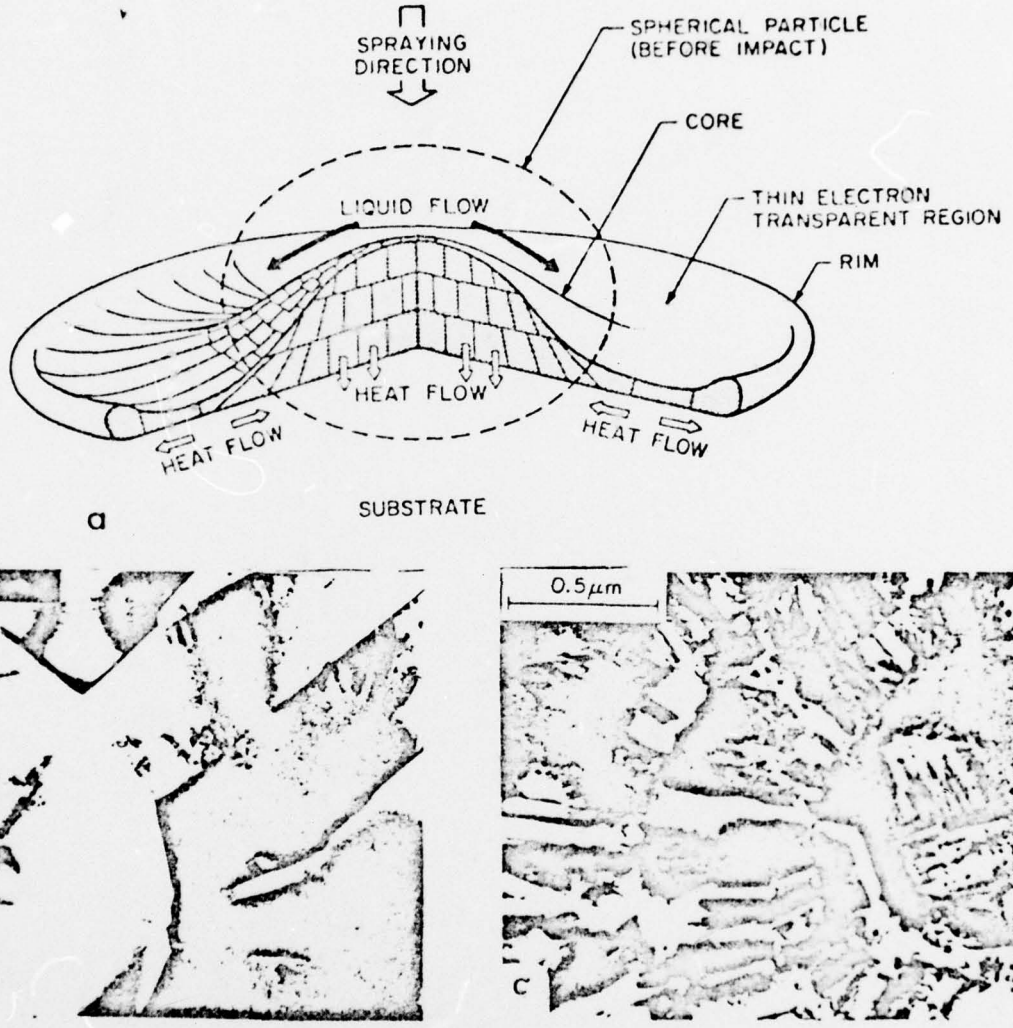

Fig. 3 – Schematic diagram of a spherical particle impinged on to a flat substrate surface (a). Transmission electron micrograph of an aluminium (b) and aluminium oxide particle (c) sprayed on to polished surfaces.

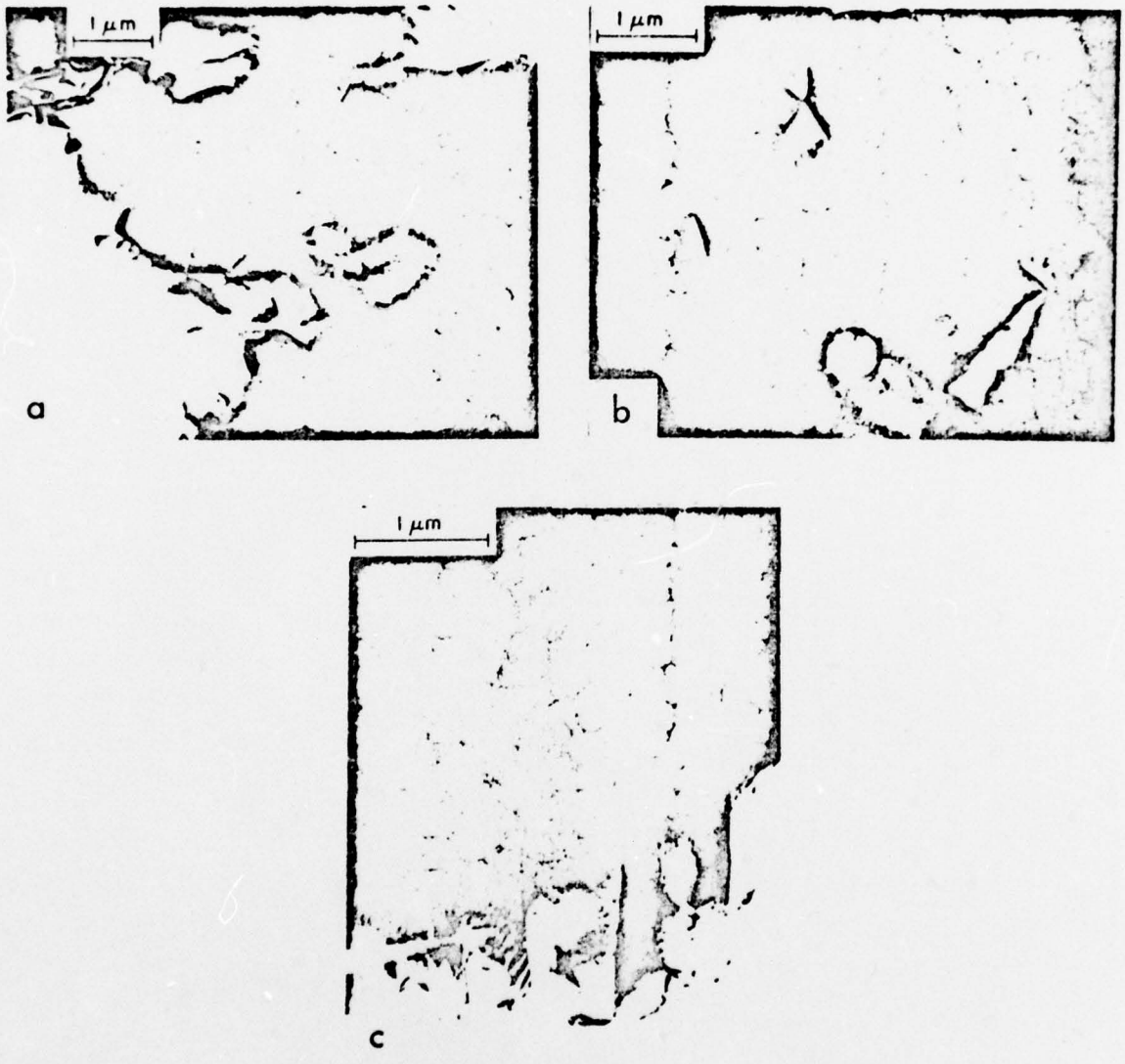

Fig. 4-Cross-sectional grain morphology in sprayed aluminium coatings showing the equiaxed grains inside (a, b) and elongated, directionally solidified regions near the substrate (c).

Fig. 5- Scanning electron micrographs of aluminium particles sprayed on to a flat surface (a) and grit blasted substrate (b). Cross-sectional view of sprayed aluminium (c) and Al_2O_3-TiO_2 coatings (d).

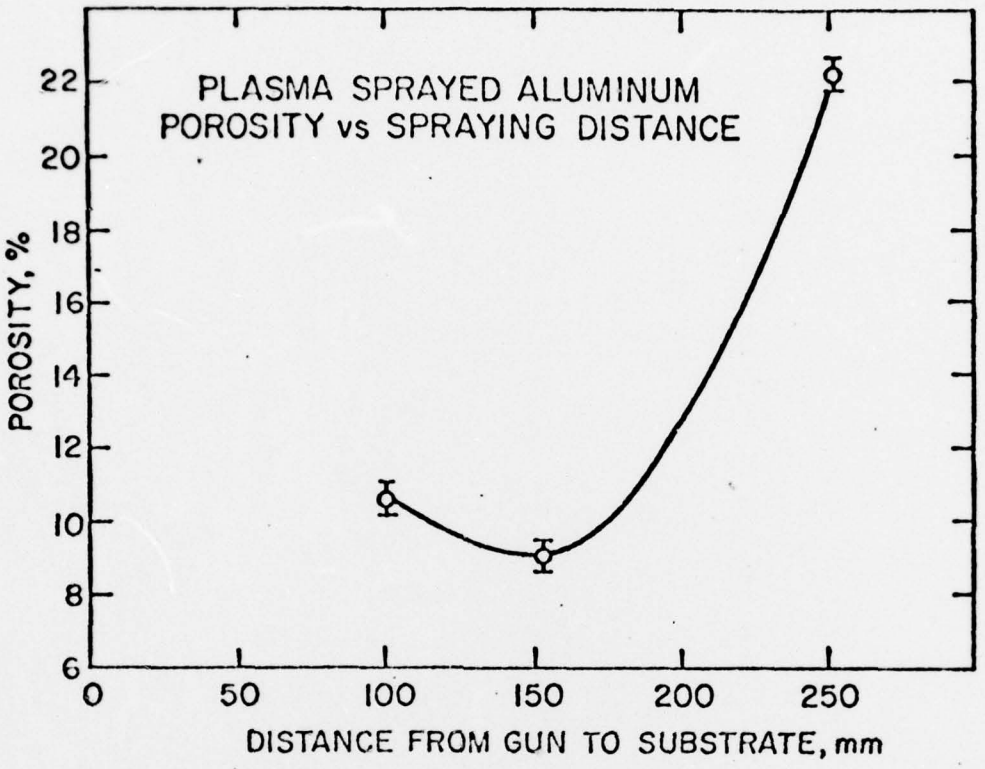
PLASMA SPRAYED ALUMINUM
POROSITY vs SPRAYING DISTANCE
POROSITY, %
22
20
18
16
14
12
10
8
6
0
50
100
150
200
250
DISTANCE FROM GUN TO SUBSTRATE, mm

Fig. 6

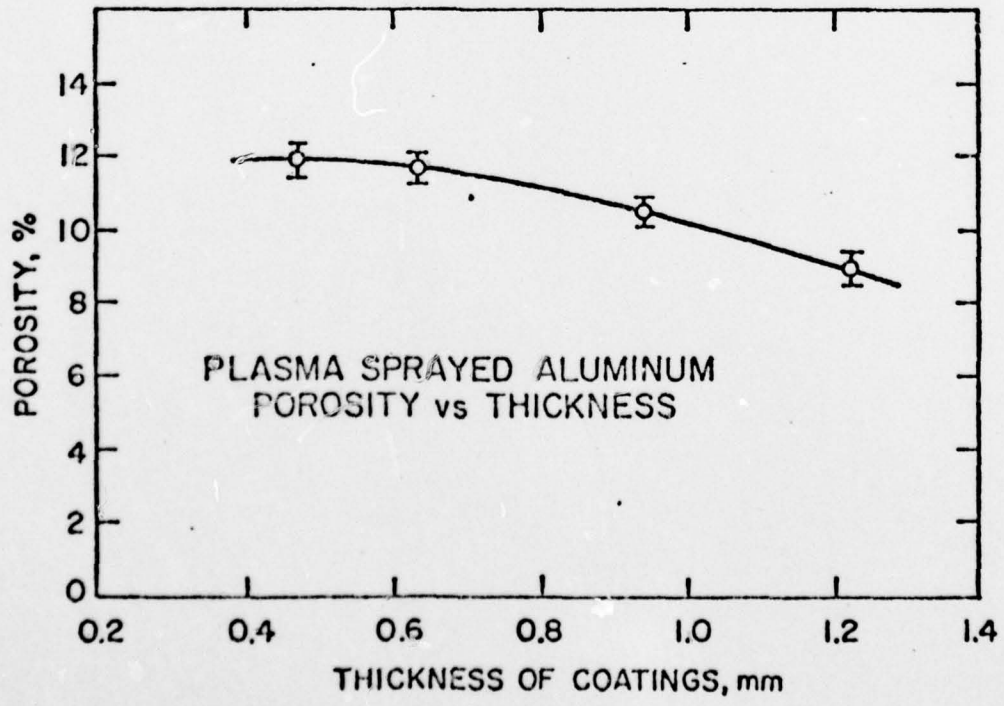
POROSITY, %
14
12
10
8
6
4
2
0
PLASMA SPRAYED ALUMINUM
POROSITY vs THICKNESS
0.2
0.4
0.6
0.8
1.0
1.2
1.4
THICKNESS OF COATINGS, mm

Fig. 7

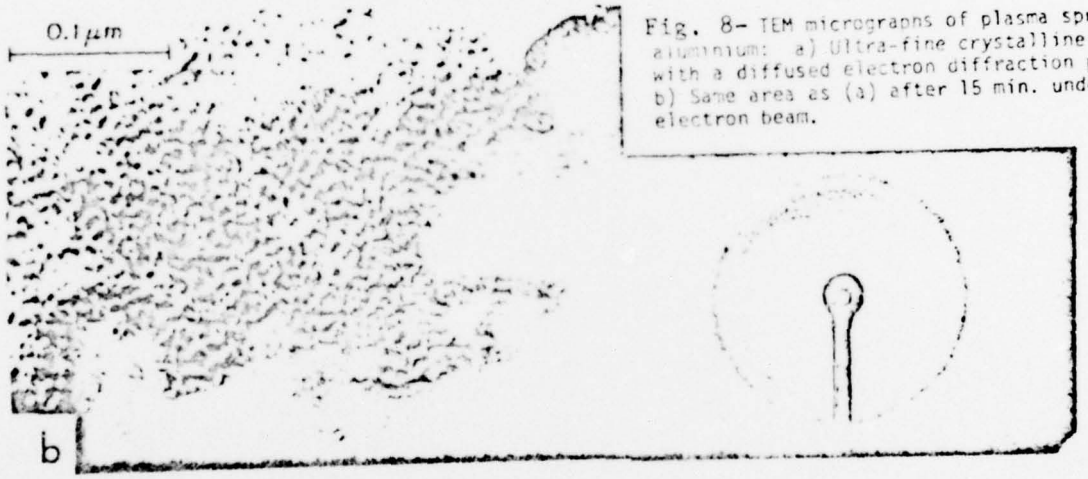

Fig. 8- TEM micrographs of plasma sprayed aluminium: a) Ultra-fine crystalline region with a diffused electron diffraction pattern. b) Same area as (a) after 15 min. under the electron beam.

c) Electrochemically thinned polycrystalline aluminium coating and the corresponding electron diffraction pattern.

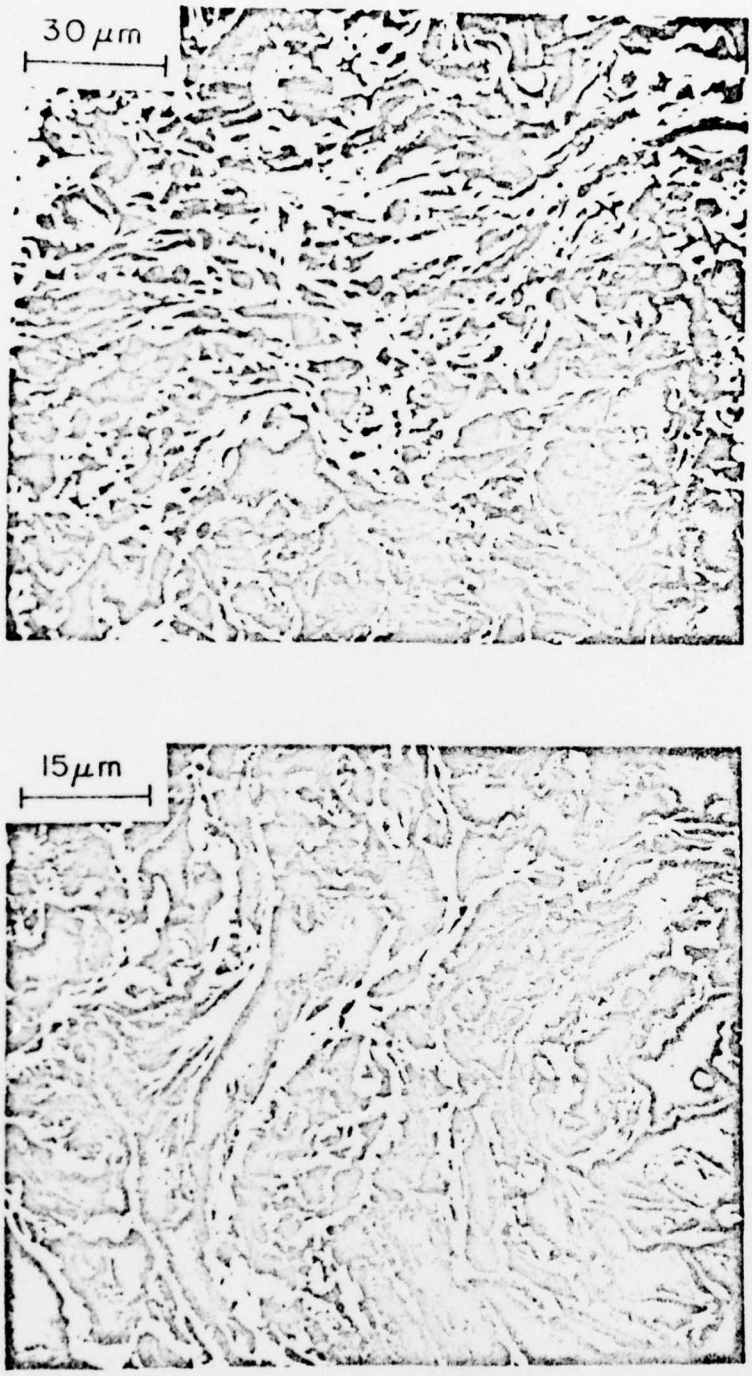

Fig. 9 - Scanning electron micrograph of a fractured aluminium coatings (3-point bending test).

Fig. 10 - TEM micrograph of sprayed aluminum-zinc alloy showing the second phase precipitate.

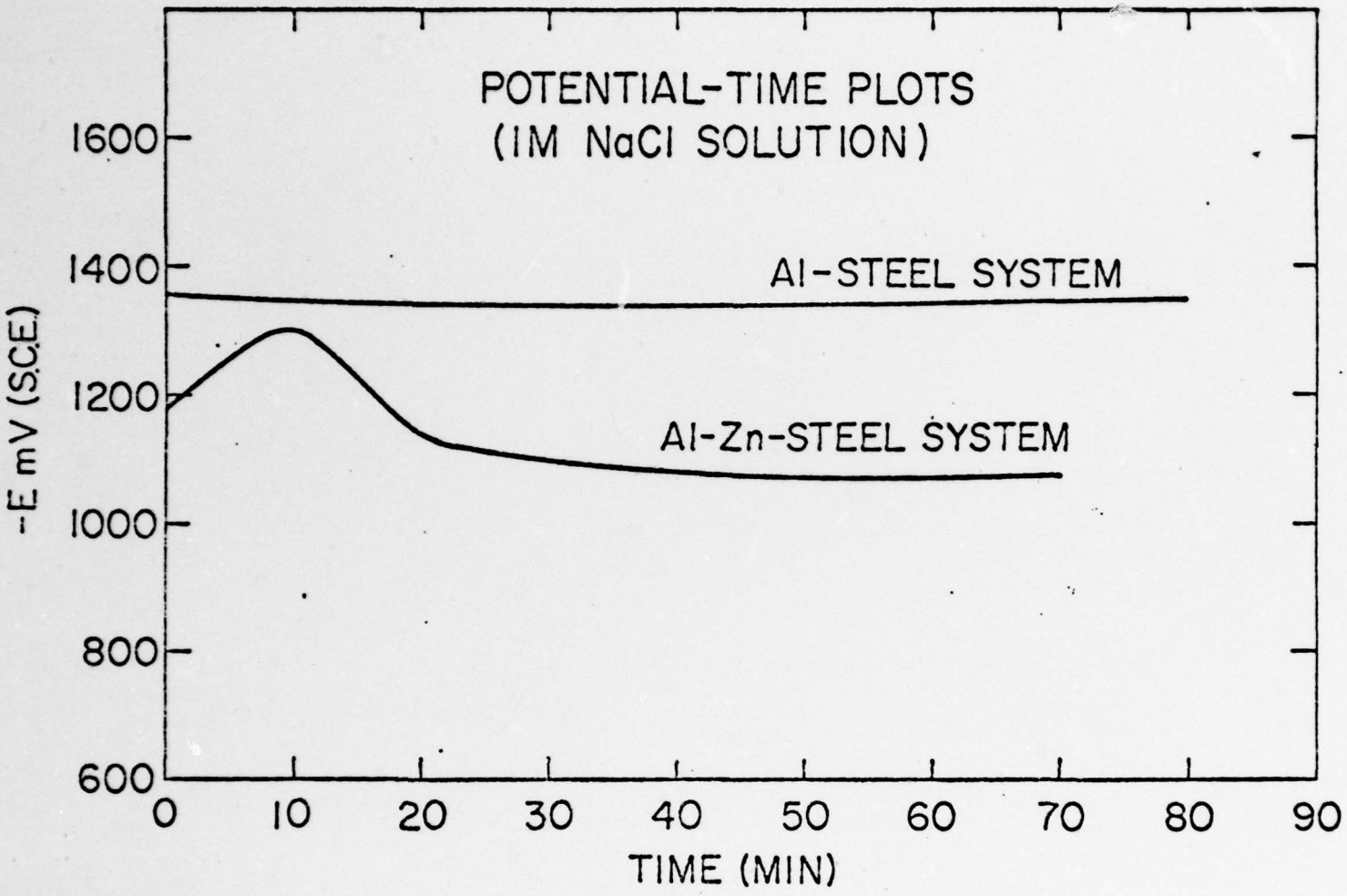
POTENTIAL-TIME PLOTS
(1M NaCl SOLUTION)
Al-STEEL SYSTEM
Al-Zn-STEEL SYSTEM
-E mV (S.C.E.)
1600
1400
1200
1000
800
600
0
10
20
30
40
50
60
70
80
90
TIME (MIN)

Fig. 11

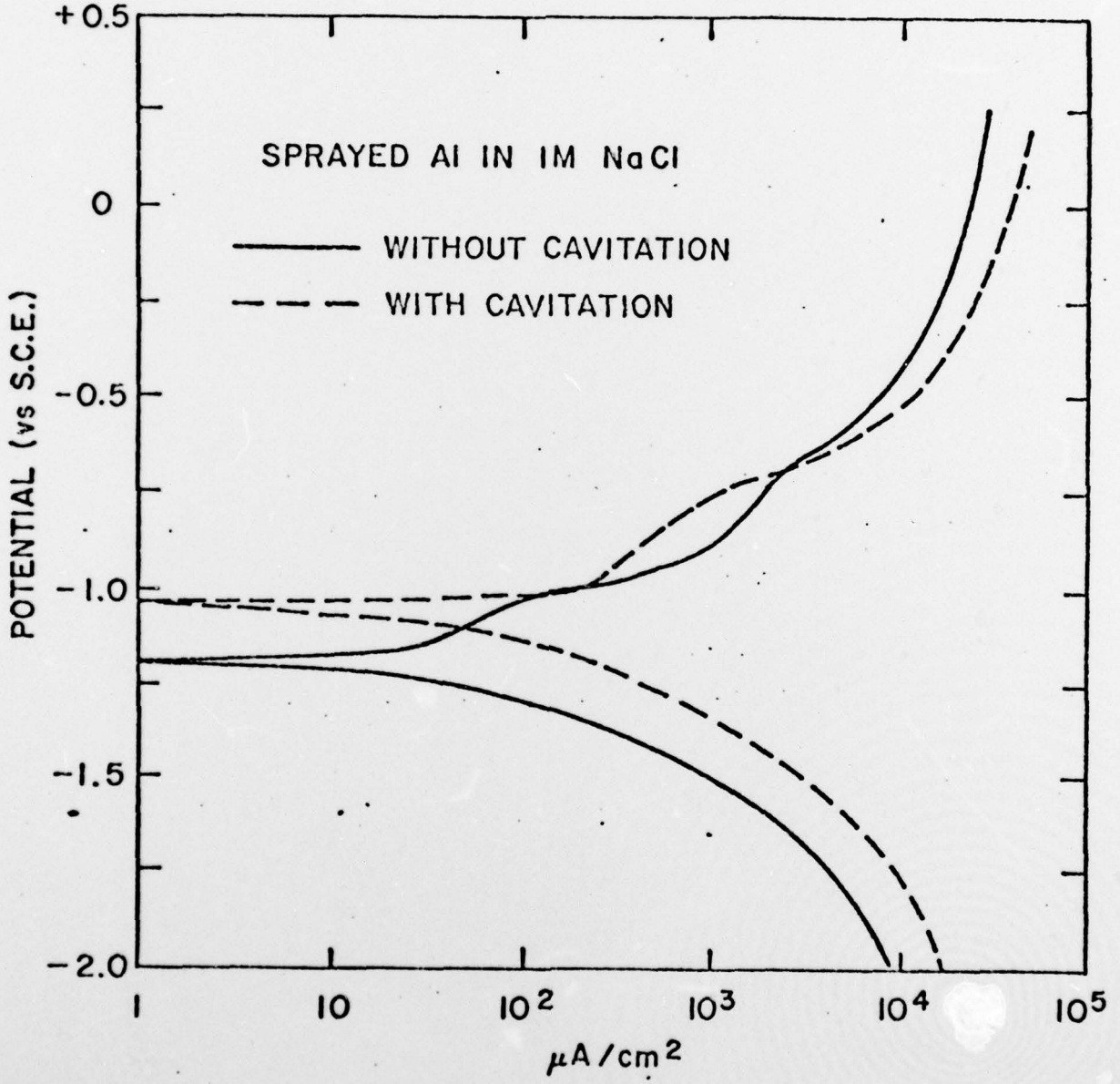
+0.5
0
-0.5
-1.0
-1.5
-2.0
POTENTIAL (vs S.C.E.)
SPRAYED Al IN IM NaCl
WITHOUT CAVITATION
WITH CAVITATION
1
10
10 2
10 3
10 4
10 5
μA/cm 2

Fig. 12

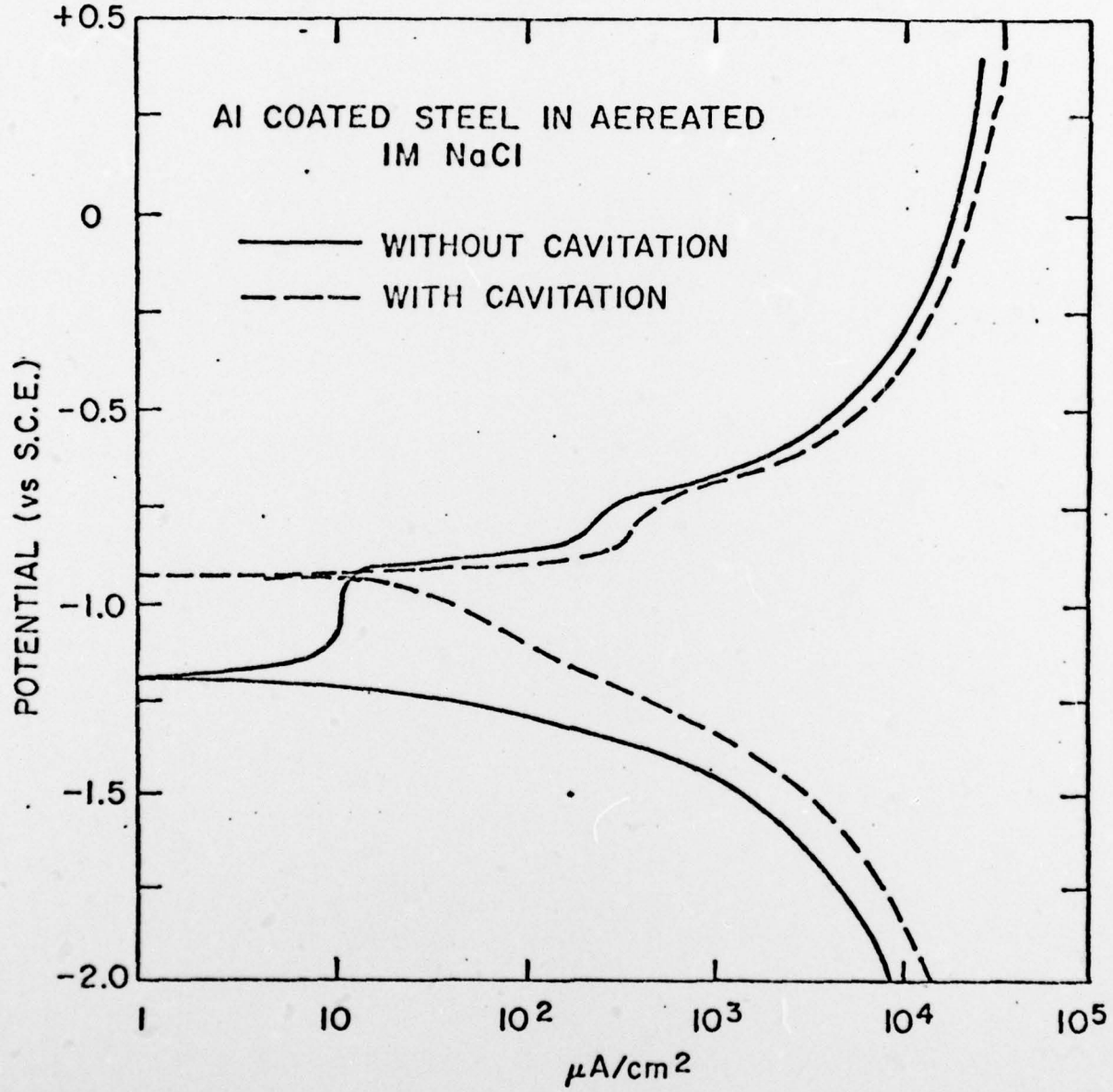
Al COATED STEEL IN AEREATED
1M NaCl
WITHOUT CAVITATION
WITH CAVITATION
+0.5
0
-0.5
-1.0
-1.5
-2.0
POTENTIAL (vs S.C.E.)
1
10
10²
10³
10⁴
10⁵
μA/cm²

Fig. 13

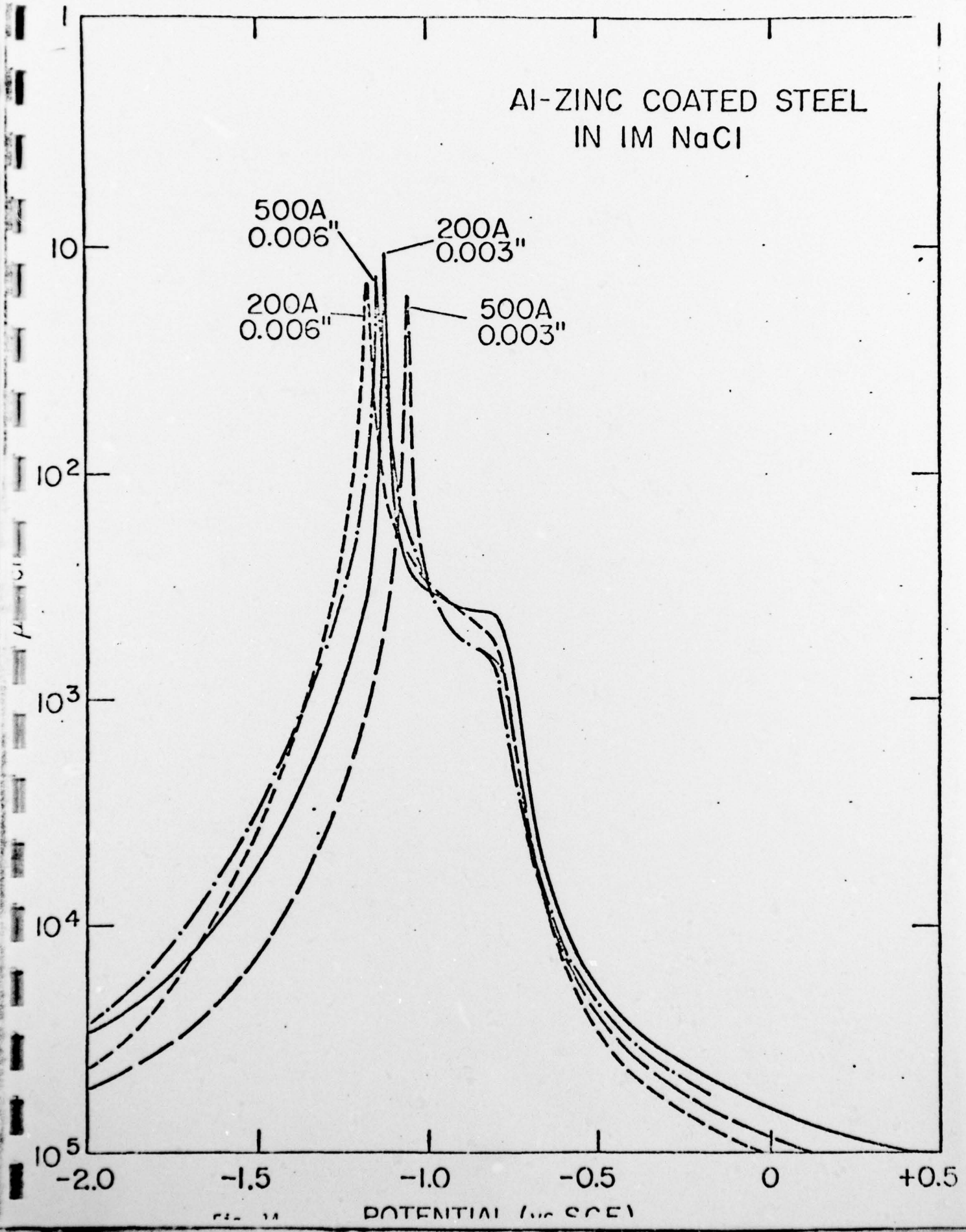
AI-ZINC COATED STEEL
IN IM NaCl
500A
0.006"
200A
0.003"
200A
0.006"
500A
0.003"
1
10
10²
10³
10⁴
10⁵
-2.0
-1.5
-1.0
-0.5
0
+0.5
POTENTIAL (vs SCE)

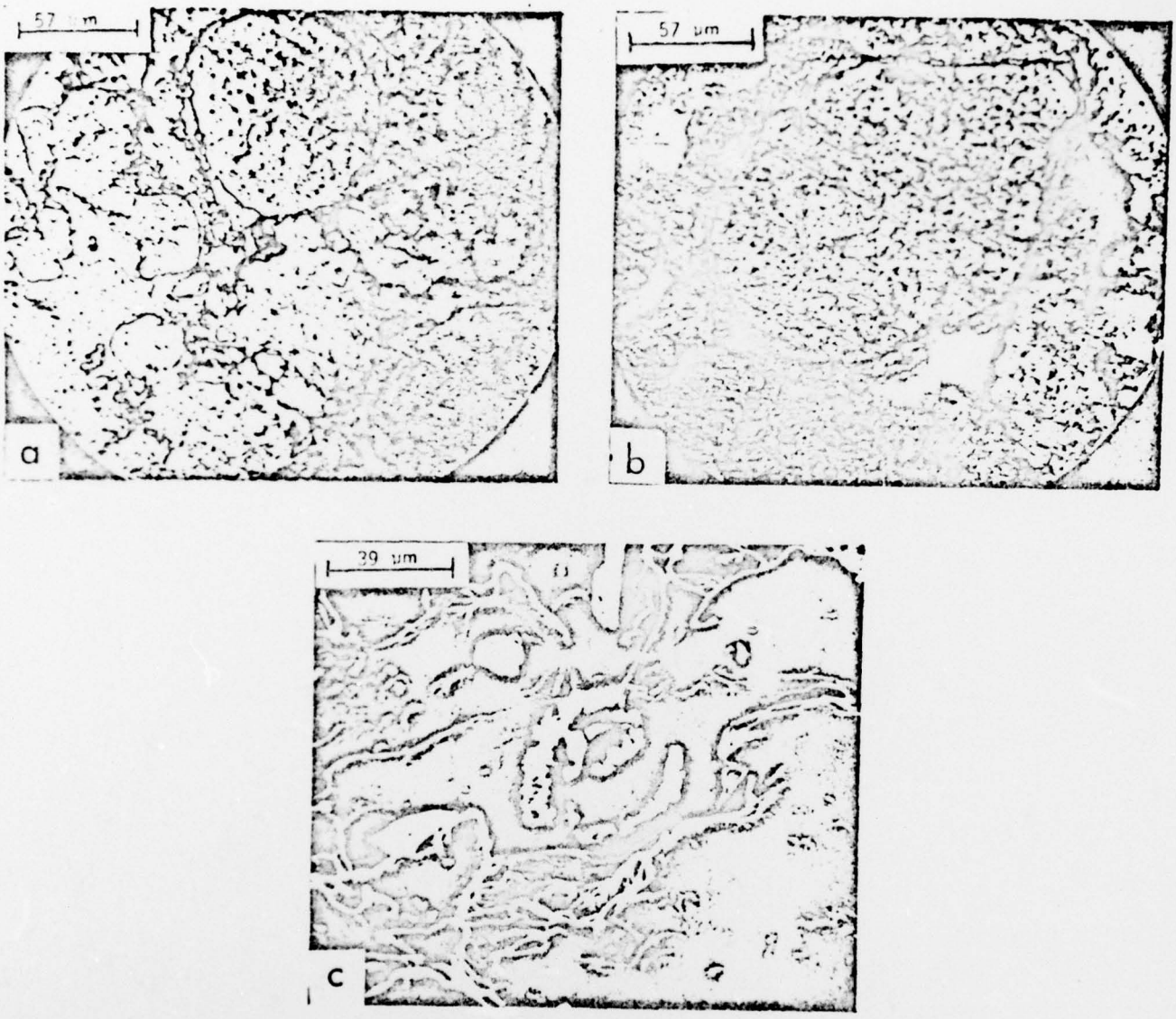

Fig. 15 - Optical micrograph of corroded sample
(a) 5 min. of corrosion (b) 10 min. of corrosion
(c) S.E.M. Micrograph of Corroded Sample showing a Pore

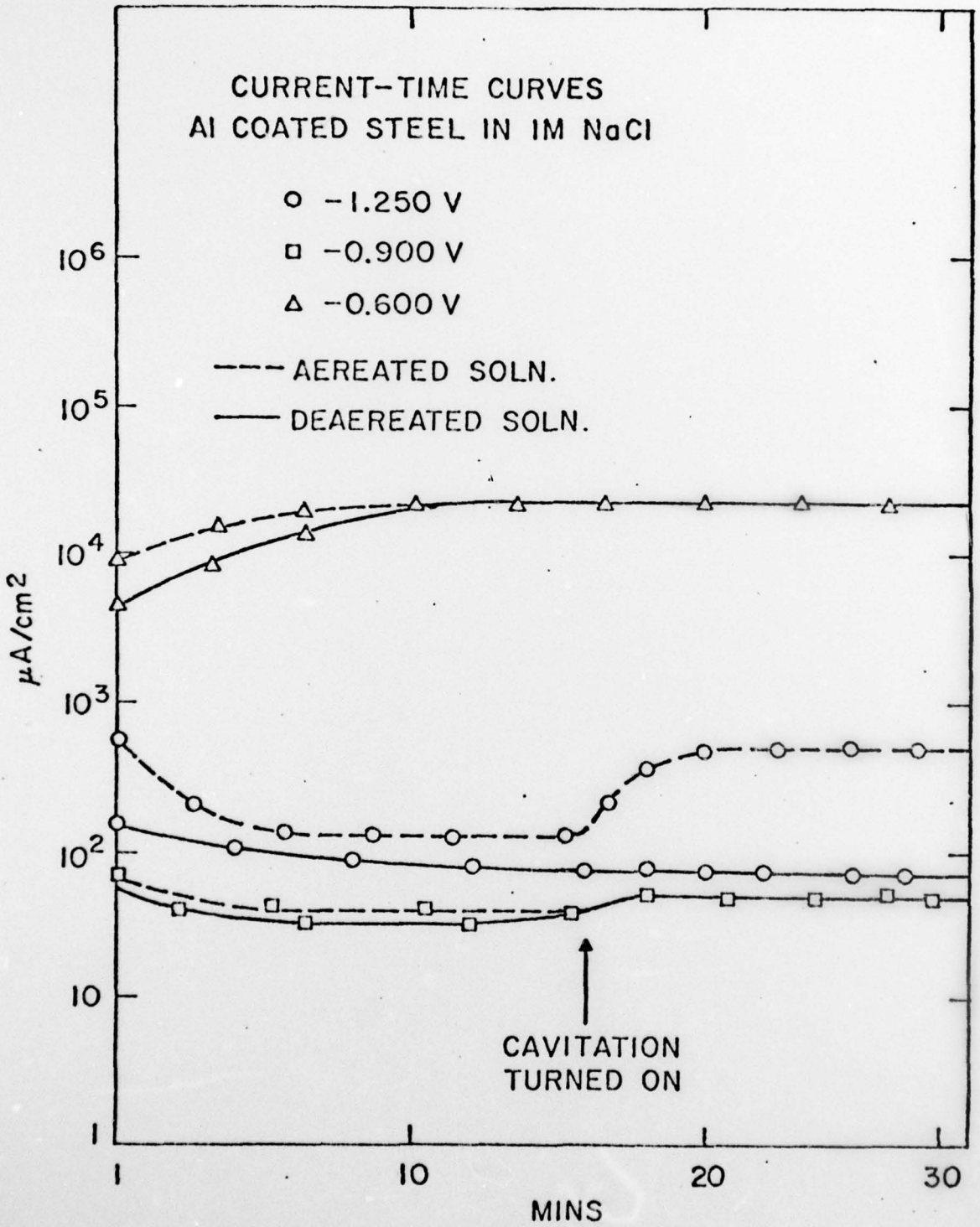
CURRENT-TIME CURVES
Al COATED STEEL IN 1M NaCl
○ -1.250 V
□ -0.900 V
△ -0.600 V
---- AEREATED SOLN.
—— DEAEREATED SOLN.
10^6
10^5
10^4
10^3
10^2
10
1
μA/cm2
CAVITATION
TURNED ON
1
10
20
30
MINS

Fig. 16

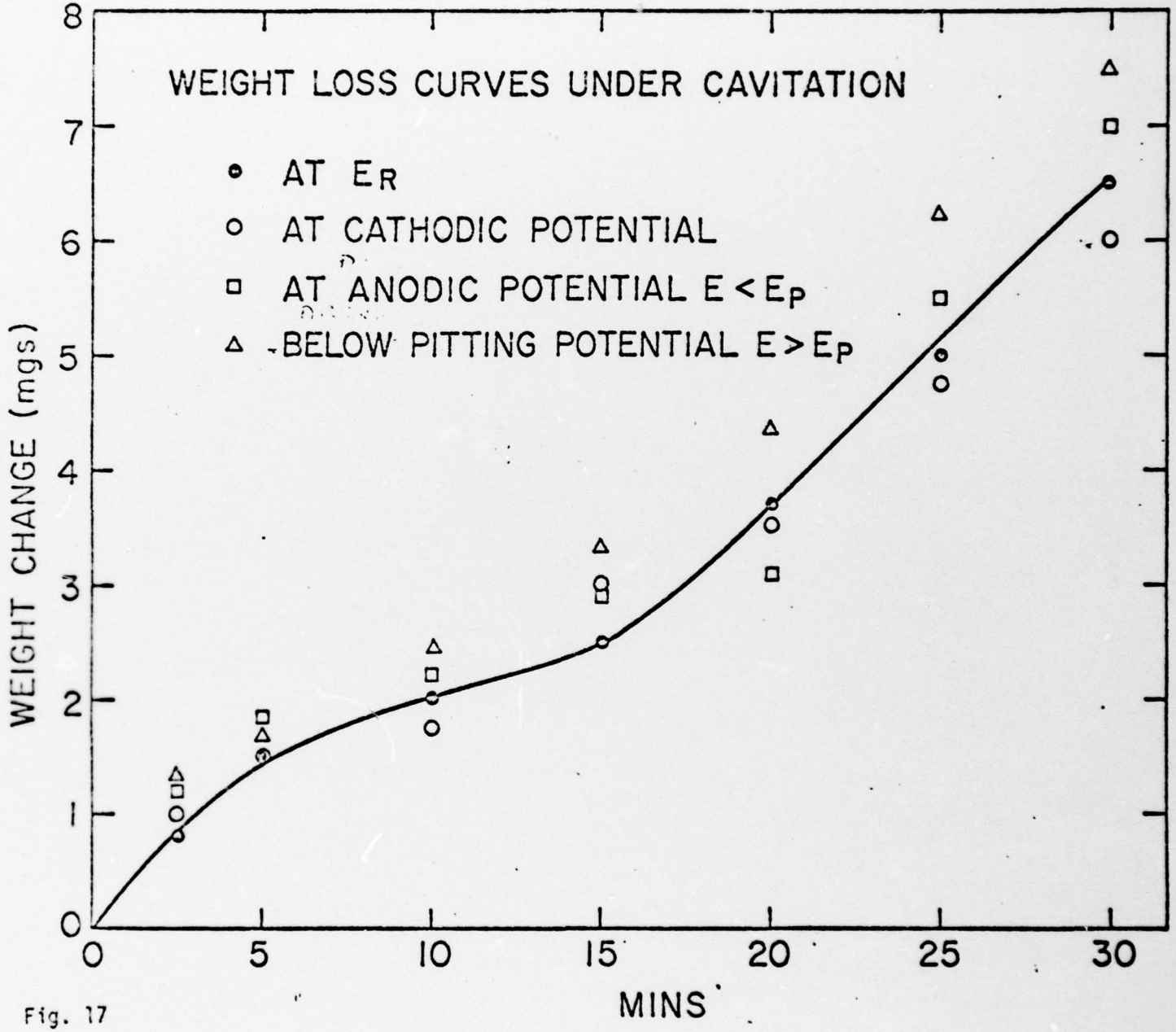
WEIGHT LOSS CURVES UNDER CAVITATION
AT E_R
AT CATHODIC POTENTIAL
AT ANODIC POTENTIAL $E < E_P$
BELOW PITTING POTENTIAL $E > E_P$
WEIGHT CHANGE (mgs)
MINS
0
1
2
3
4
5
6
7
8
0
5
10
15
20
25
30

Fig. 17

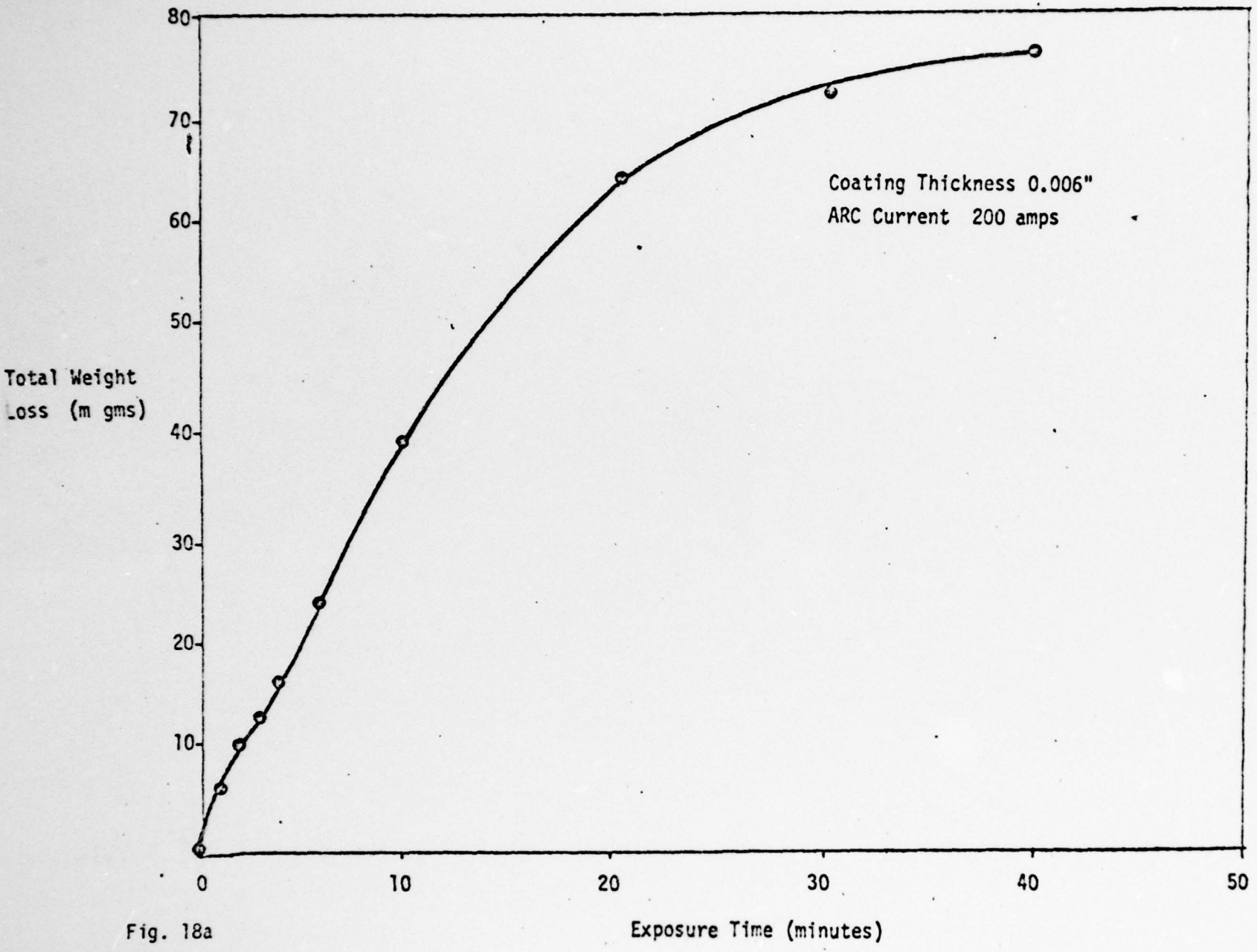
80
70
60
50
40
30
20
10
0
10
20
30
40
50
Coating Thickness 0.006"
ARC Current 200 amps
Total Weight Loss (m gms)
Exposure Time (minutes)

Fig. 18a

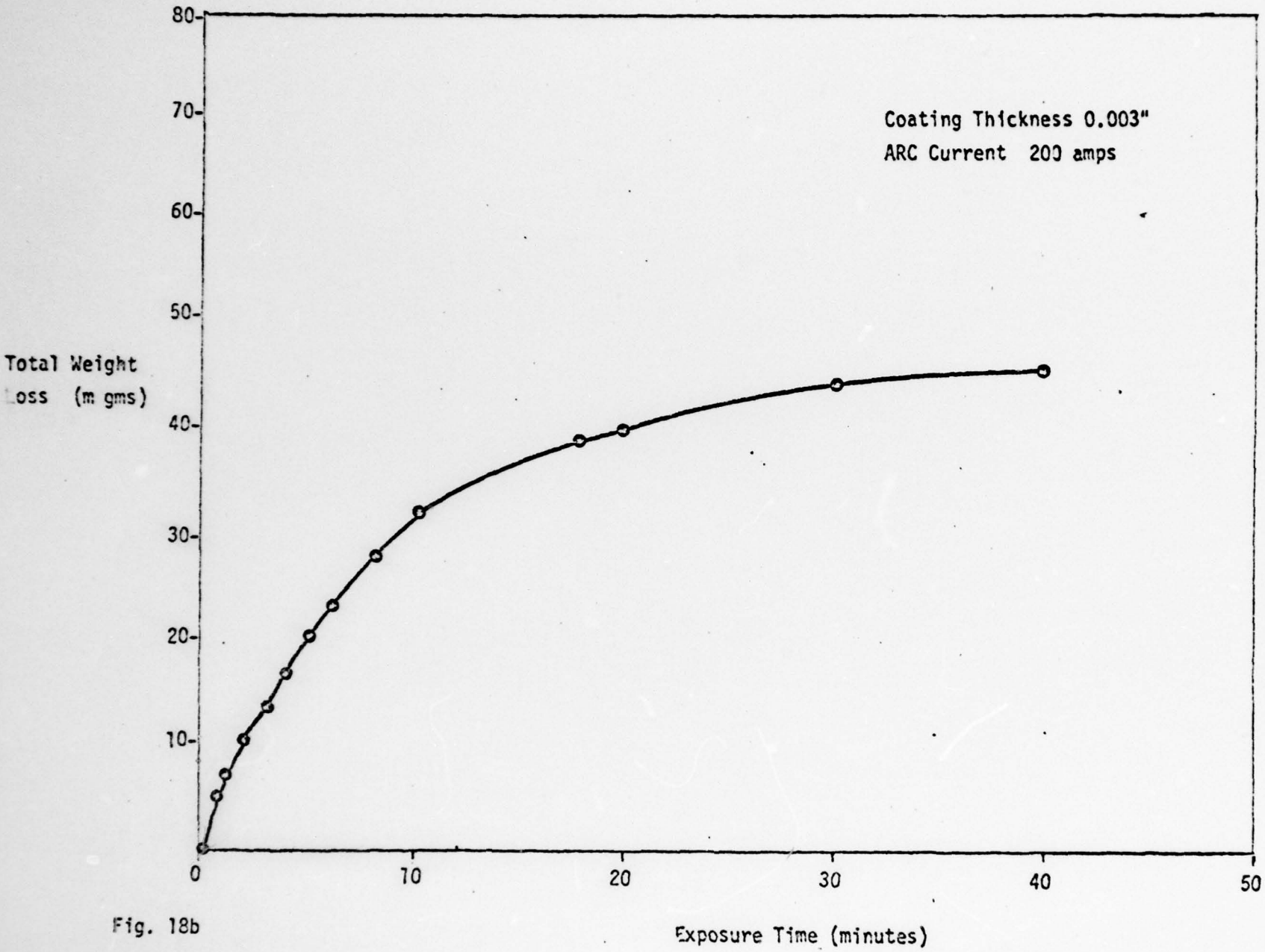
Coating Thickness 0.003"
ARC Current 200 amps
Total Weight Loss (m gms)
80
70
60
50
40
30
20
10
0
10
20
30
40
50
Exposure Time (minutes)

Fig. 18b

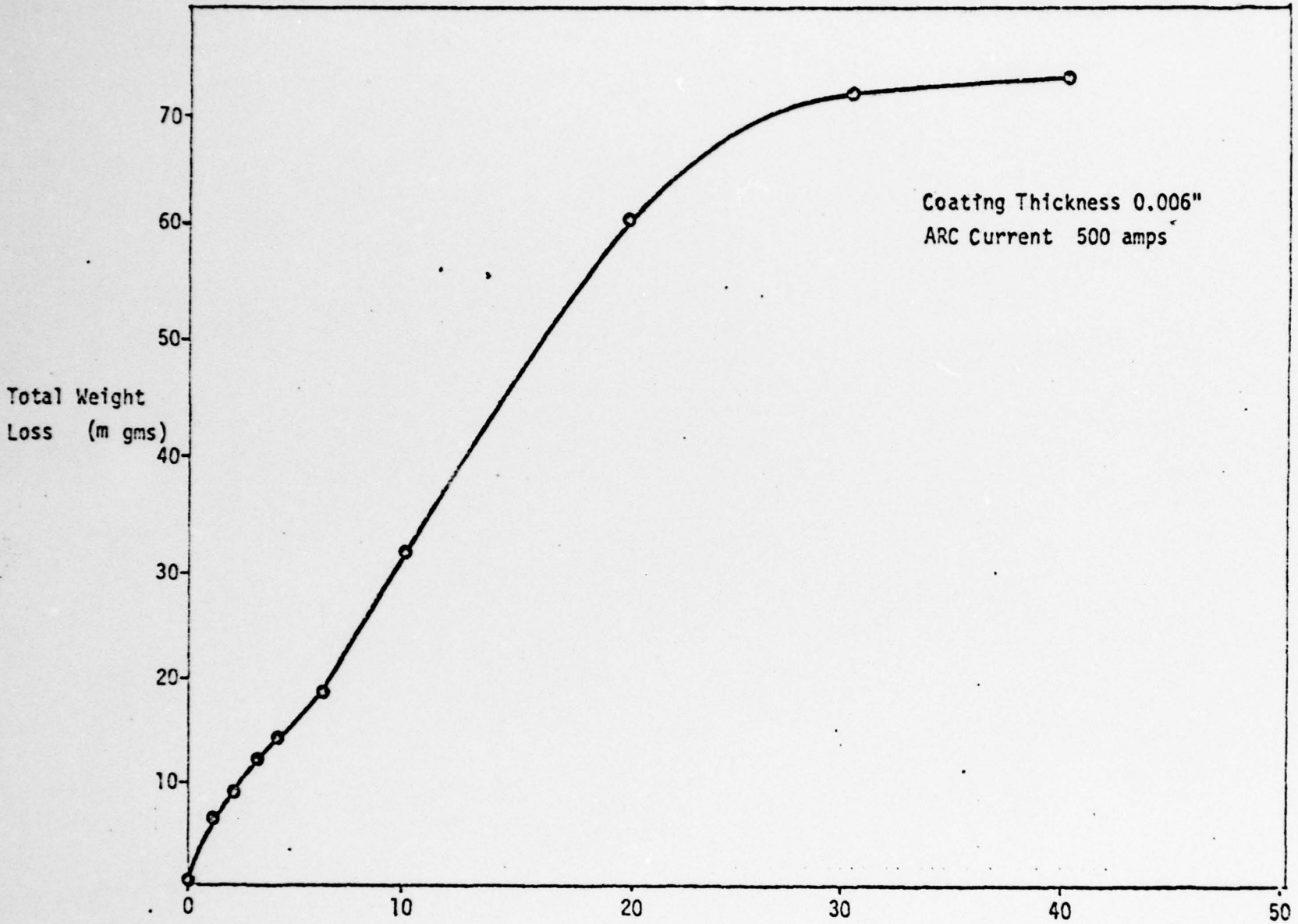
Coating Thickness 0.006"
ARC Current 500 amps
Total Weight Loss (m gms)
70
60
50
40
30
20
10
0
10
20
30
40
50
Exposure Time (minutes)

Fig. 18c

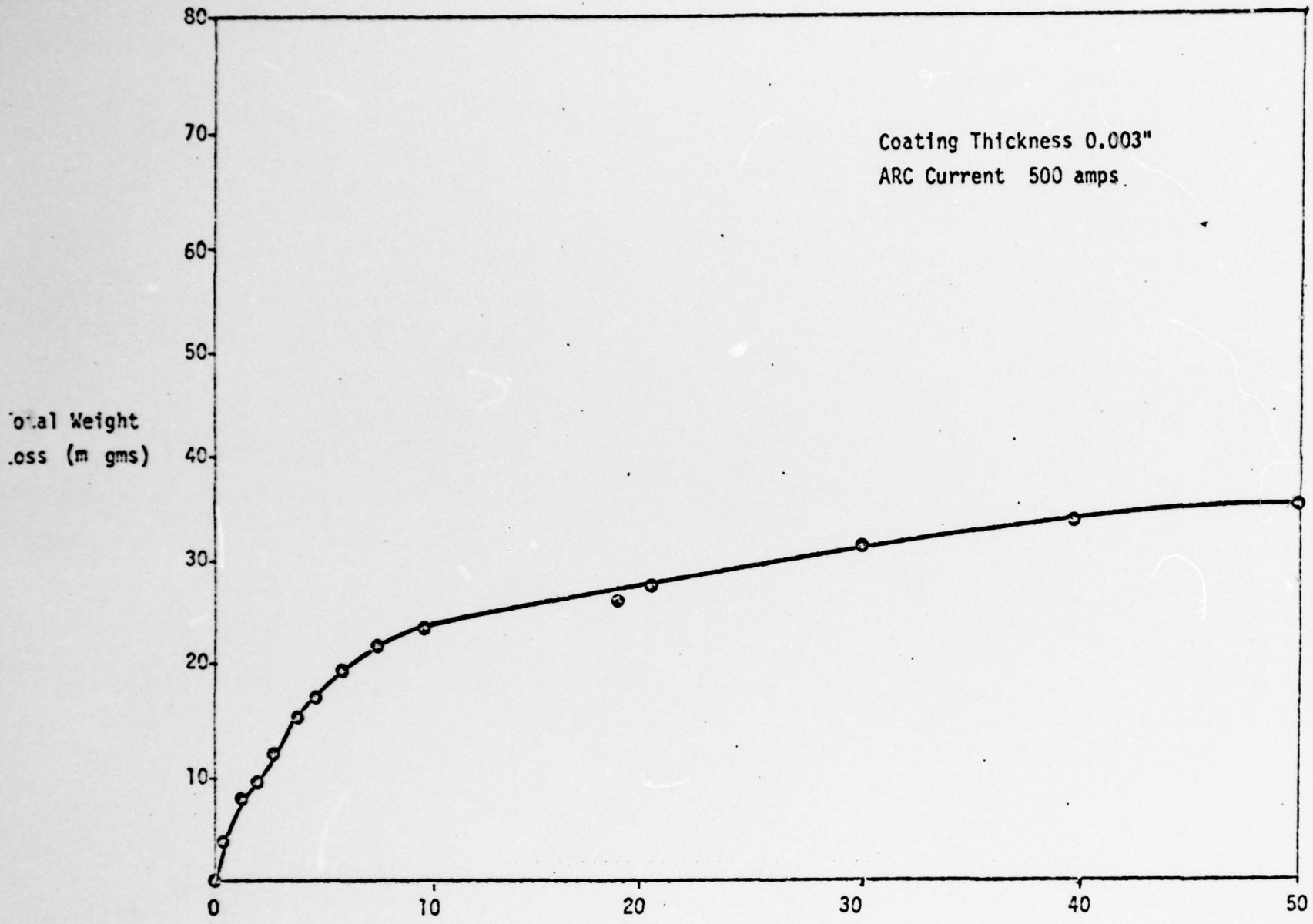
Coating Thickness 0.003"
ARC Current 500 amps
80
70
60
50
40
30
20
10
0
10
20
30
40
50
Total Weight Loss (m gms)
Exposure Time (minutes)

Fig. 18d

Fig. 19 - S.E.M Micrographs of Electric Arc sprayed Zn-15wt% Al
(a) as sprayed coating (b) 30 secs of cavitation
(c) 60 secs of cavitation (d) 3 minutes of cavitation

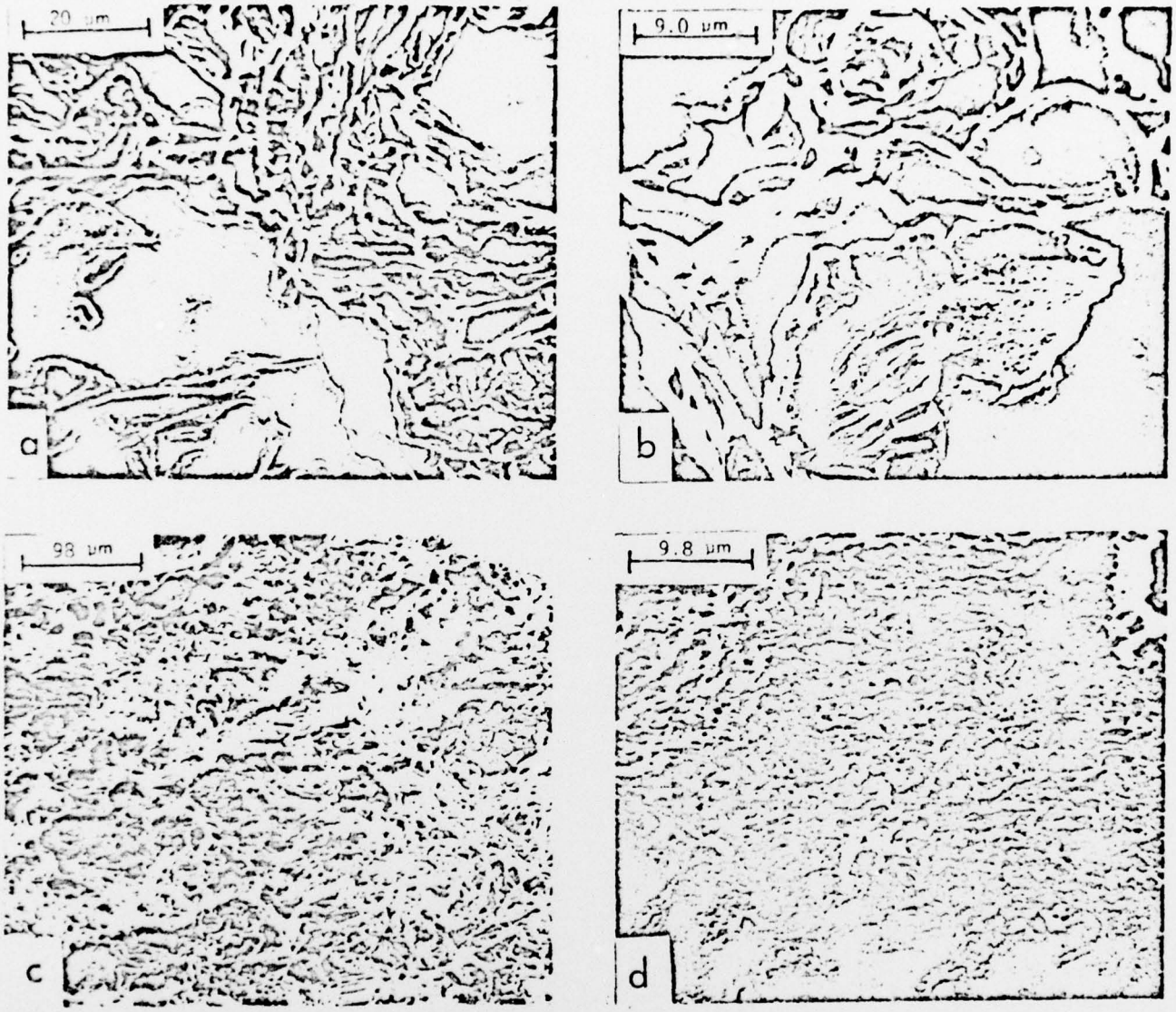

Fig. 20 - S.E.M. Micrograph of Electric Arc sprayed Zn-15wt% Al
(a) 5 min. of cavitation (b) Magnified view of (a)
(c) 10 min. of cavitation (d) magnified view of (c)